K. Capacitor Technologies for Power Electronic Systems

D.Y. Kaufman, S.K. Streiffer, O. Auciello, M.T. Lanagan,[†] and U. Balachandran
Energy Technology and Materials Science Divisions
Argonne National Laboratory, Argonne, IL 60439
(630)252-4250 e-mail: balu@anl.gov

[†]Center for Dielectric Studies, Pennsylvania State University

---

Objectives

- Develop advanced capacitor technologies to reduce the size, weight, and cost of power electronic modules.

Approach

- Develop microelectronic-scale ferroelectric thin film (<1 μm) capacitors with high dielectric constant and high electric field breakdown strength for use as discrete and integrated capacitors.

- Develop antiferroelectric/ferroelectrics phase switch materials with significant energy storage capability.

- Collaborate with capacitor companies to identify technologies to meet objectives and supply prototype capacitors to high-power inverter manufacturers for reliability and performance studies.

Accomplishments

- Used semiconductor production techniques to fabricate barium strontium titanate (BST) thin film capacitors with dielectric constants of 580, dielectric losses as low as 0.003, and breakdown fields of 3-4 MV/cm.

- Developed antiferroelectric/ferroelectrics phase switch materials with a 100% improvement in high field dielectric constant over typical multilayer ceramic capacitor materials.

- Incorporated multilayer ceramic capacitors in a 100 kW inverter (collaboration with AVX Corporation and Oak Ridge National Laboratory) and an output filter for a 150 kW 1450 V-peak voltage power inverter (collaboration with AVX Corporation and Angelo Ferraro).

Future Directions

- Develop capacitor architectures and processing schemes to arrive at a robust commercial fabrication methodology for thin film capacitors.
- Characterize the temperature dependent reliability of prototype capacitors fabricated in collaboration with capacitor manufacturers.
- Develop low cost base-metal electrode technologies to reduce capacitor cost

---

Introduction

Advanced power electronic modules require low cost capacitors with reduced weight and size. Work at Argonne National Laboratory, in collaboration with the Center for Dielectric Studies at Penn State, has focused on developing ferroelectric ceramics that can achieve the high charge and energy densities necessary for these components (Figure 1).

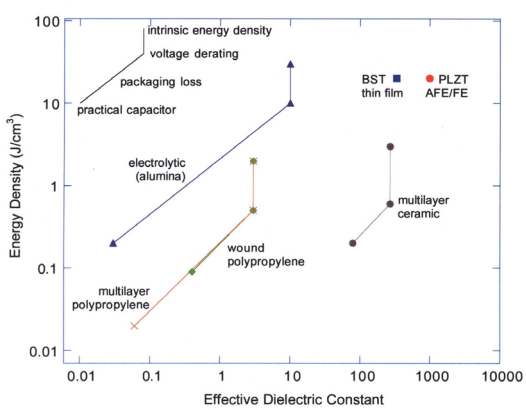

Figure 1. Comparison of the energy density of various capacitor technologies. BST thin films and PLZT AFE/FE materials show promising initial results and are expected to achieve even higher energy densities with continued process development.

Two technologies are being pursued: 1) barium strontium titanate ($Ba_{1-x}Sr_xTiO_3$, annotated as BST) thin film capacitors and 2) lead lanthanum zirconate titanate ($Pb_{1-x}La_x(Zr_yTi_{1-y})O_3$, annotated as PLZT), antiferroelectric/ferroelectric (AFE/FE) switching materials.

BST Thin Film Capacitors

High volumetric efficiency can be achieved by miniaturization of the capacitors to microelectronic scale dimensions. Besides serving as discrete components such capacitors could be integrated directly onto silicon-based switching circuits, reducing component footprint and the number of assembly steps. BST combines the best choice of dielectric properties and ease of fabrication. Vapor deposited thin films exhibit better materials uniformity, higher density, and smother interfaces than their bulk/thick film counterparts. As a result, higher breakdown fields, and consequently higher charge storage and energy densities, can be obtained.

Capacitors were fabricated by two thin film techniques extensively used in the microelectronics industry, metalorganic chemical vapor deposition (MOCVD) and magnetron sputtering. Prototype capacitors were fabricated by depositing 100-200nm BST films on silicon substrates with a platinum electrode layer (Figure 2). Microstructural characterization of the BST dielectric film was performed to determine the composition, morphology, and

crystallographic orientation of the film. Discrete capacitors were then formed by evaporating platinum top electrodes, and the dielectric properties of the films characterized.

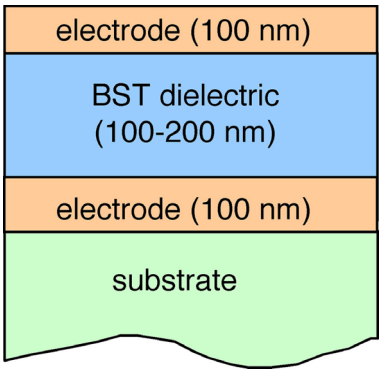

Figure 2. Schematic diagram of a single layer BST thin film capacitor.

ANL has designed a novel MOCVD reactor which includes a commercial chemical delivery tool (ATMI LDS-300B) (Figure 3). Metalorganic solutions of the constituent elements are metered to a vaporizer and the resulting gas stream is carried into the reactor and dispersed over the heated substrate to react and form the solid thin film. This deposition scheme allows strict control of the film composition and excellent compositional and thickness uniformity over large areas.

The effect of film composition, growth conditions, and post-processing annealing were investigated and correlated with electrical properties. Titanium rich films ((Ba+Sr)/Ti=0.96) displayed lower leakage and were therefore more extensively investigated. Appropriate growth conditions were determined for deposition of {001} uniaxially oriented polycrystalline BST thin films. Post processing annealing of the capacitors dramatically reduced the dielectric loss by 69% to 0.003 and extended the onset of leakage. The mechanisms responsible, including improvement of the chemistry and structure of the dielectric-electrode interface, and filling of oxygen

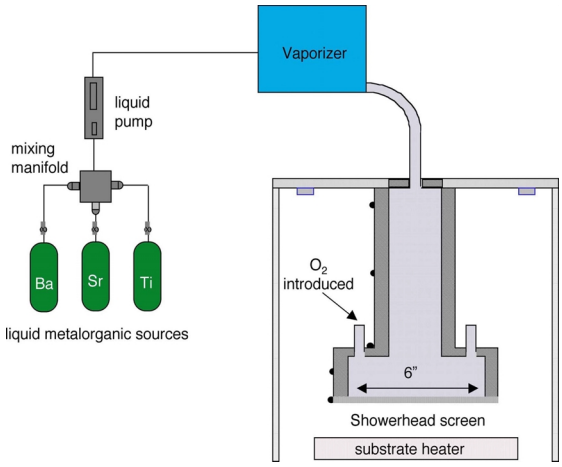

Figure 3. Schematic diagram of the metalorganic chemical vapor deposition (MOCVD) system (ATMI precursor delivery system and ANL reactor)

vacancies in the dielectric, are being investigated.

Dielectric constants of 580 (yielding a thin film layer with a capacitance per unit area of 4.3 $\mu F/cm^2$) at zero bias and 178 (1.3 $\mu F/cm^2$) at an electric field of 0.4 MV/cm have been obtained. Breakdown fields of 2.6 MV/cm have been achieved. These dielectric properties lead to energy densities as high as 21 J/cm^3 for the dielectric film. Higher dielectric properties and energy densities are expected with continued process development.

BST thin films were also deposited by magnetron sputtering. Both the Ba/Sr and (Ba+Sr)/Ti ratios could be varied as a function of the total deposition pressure, and had a dramatic result on the film crystallinity and dielectric properties. Near stoichiometric films were polycrystalline and possessed high dielectric constants of 560. Titanium rich films, which were nanocrystalline to amorphous, exhibited

reduced dielectric losses to as low as 0.005, but much reduced dielectric constants of 150 and lower. We have developed methods for the deposition of multilayer thin films with changes in composition and microstructure for the different layers. This approach is very promising and has allowed us to maintain a high dielectric constant of approximately 300 with losses as low as 0.005 and breakdown fields of 3-4 MV/cm. Optimization of the multilayers is still being studied.

Antiferroelectric/Ferroelectric (AFE/FE) Capacitors

Ferroelectric barium titanate based thick film multilayer ceramic capacitors (MLCCs) have gained commercial significance in terms of higher total energy storage densities and lower costs due to many advances in fabrication technology. However, there is growing interest in exploring the high-energy storage potential of materials which undergo phase switching from the antiferroelectric to the ferroelectric (AFE/FE) state. On application of an electric field, AFE/FE materials exhibit high-induced polarization thereby storing and recovering large amounts of specific energy. The most promising AFE/FE system is lead lanthanum zirconate titanate (PLZT). Dielectric and polarization measurements were performed on single layer PLZT capacitors with different compositions (TRS Ceramics, Inc.). The high field permittivity of PLZT AFE/FE materials exceeded that of commercial barium titanate materials by 100% (Figure 4). Additionally, the stored energy of these capacitors was ~5 times higher than that of polymer based polystyrene capacitors. We are continuing to collaborate with TRS Ceramics Inc. to fabricate and test multilayer PLZT AFE/FE ceramic capacitors.

Ceramic Capacitor Demonstration

Volume efficient ceramic capacitors were incorporated into two demonstration projects. In collaboration with AVX Corporation and ORNL, multilayer ceramic capacitors were substituted for multilayer polymer capacitors in a 100 kW inverter.

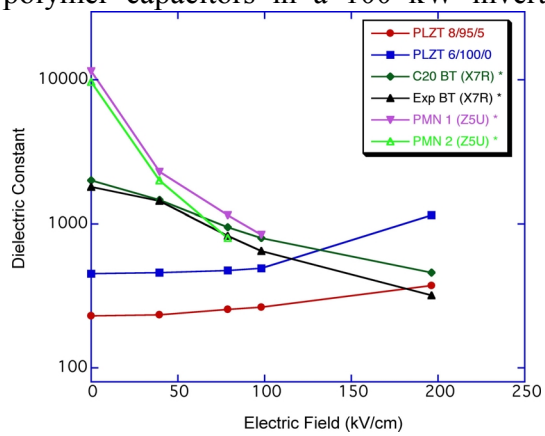

Figure 4. Plot of dielectric constant with applied field for commercial dielectrics (PMN1, PMN2, C20BT, Exp BT) and PLZT AFE/FE materials.

The new capacitors were six times smaller than the original capacitors. In collaboration with Angelo Ferraro and AVX Corporation, multilayer ceramic capacitors were substituted for wound polymer capacitors in an output filter for the U. S. Navy 150-kW inverter demonstration. Evaluation of the demonstration systems is still being performed.

Publications

"High-Dielectric-Constant Ferroelectric Thin Film and Bulk Ceramic Capacitors for Power Electronics", D. Y. Kaufman, M. T. Lanagan, J. Im, P. Baumann, R. A. Erck, J. Giumarra, S. K. Streiffer, O. Auciello, M. J. Pan, P. Baldo, and J. Zebrowski, Proceedings of the PCIM '99 Power Electronics Conference, November 1999, Chicago, IL, pg. 317.

"Composition-Control of Magnetron-Sputter-Deposited $Ba_xSr_{1-X}Ti_yO_{3+z}$Thin Films for Voltage Tunable Devices", J. Im, O. Auciello, P. K. Baumann, S. K. Streiffer, D. Y. Kaufman, and A. R. Krauss, Applied Physics Letters, Vol. 76, pg. 625, 2000.

L. Nanostructure Multilayer Materials for Capacitors

Troy W. Barbee, Jr., L-350
Lawrence Livermore National Laboratory, Livermore CA, 94550-9234
(925) 423-7796: fax; (925) 422-6892: e-mail; barbee2@llnl.gov

---

Objectives:

- Develop a physical vapor deposition process to fabricate high energy density capacitors for electrical power control applications.
- Develop low loss moderate ($10 < k < 30$) to high ($30 < k < 100$) dielectric constant materials.
- Fabricate demonstration capacitors that have required application defined performance.
- Technology transfer developed capacitor fabrication process to industry.

Approach:

- Endeavor to develop a capacitor fabrication physical vapor technology compatible with semiconductor fabrication processing.
- Apply high deposition rate precision reactive magnetron sputter deposition technology to capacitor fabrication process development.
- Develop high energy density capacitor performance by means of high breakdown fields rather than by use of very high dielectric constant materials
- Develop low loss moderate ($10 < k < 30$) to high ($30 < k < 100$) dielectric constant materials exhibiting high breakdown fields and low dependence of performance on temperature.

Accomplishments:

- Developed high device yield reactive magnetron sputtering fabrication process for high energy density capacitor fabrication. (3 United States patents granted: no. 5,414,588; no. 5,486,277; no. 5,742,471).
- Applied high device yield reactive magentron sputtering fabrication process to the fabrication of capacitors using dielectric materials having dielectric constants of 9 to 41.

- Experimentally demonstrated that reactive magnetron sputter deposition fabricated nanostructure multilayer material capacitors can be low loss and exhibit low temperature dependence.

- Demonstrated that the observed breakdown fields are a systematic function of the dielectric constants, decreasing as the dielectric constants increase.

- Initiated technology transfer process: published *Commerce Business Dai*ly advertisement to develop manufacturing concern interest – currently negotiating content with selected commercial partner.

Future Directions:

- Continue development of high breakdown strength low-loss low-temperature dependence dielectric materials to increase performance of nanostructure multilayer material capacitors.

3. ADVANCED MATERIALS FOR POWER ELECTRONICS

A. Carbon Foam Thermal Management Materials for Electronic Packaging

James Klett, Lynn Klett, Tim Burchell, Claudia Walls
Oak Ridge National Laboratory, Oak Ridge TN, 37831-6087
(865) 574-5220; fax: (865) 574-6918; e-mail: klettjw@ornl.gov

---

Objectives

- Collaborate with potential manufacturers with regard to designing, testing, and manufacturing of smaller, lighter, and more efficient heat exchangers and heat sinks for power electronics, utilizing the high conductivity carbon foam.
- Utilize improved understanding of effects of processing conditions on foam structure to increase the thermal conductivities of high conductivity carbon foams by more than 50%.

Approach

- Vary processing conditions and characterize foam structures to gain understanding of effects of process conditions on structures that affect thermal properties.
- Work with industrial partners to define targets for foam-based heat exchangers.
- Develop joining/bonding techniques to laminate the foam to heat exchangers without sacrificing thermal conductivity.

Accomplishments

- Met program goal for increasing thermal conductivity by over 50%.
- Licensed the technology to Poco Graphite, Inc. to commercialize the material and scale up for production for large volume markets.
- Developed bonding techniques with both epoxies and brazing for laminating foam to different materials.
- Developed electroplating technique for improving the surface ruggedness of the foam.

Future Direction

- Develop logic and system design for integration of the foam into application-specific devices.
- Improve understanding of pressure drop/density/thermal conductivity/heat transfer coefficient relationships to ensure optimum weight-efficiency tradeoffs.
- Increase heat flux/weight by up to 10-fold.

Introduction

Two devices are currently used for thermal management: heat exchangers, which transfer heat energy from one area of a device to another; and heat sinks, which dissipate heat into the air. Currently, most cooling heat exchangers for high-power electronics use layers of water-cooled aluminum or copper plate mounted below the electrical circuitry to transfer heat from hotter areas to cooler areas. Using carbon foam as the core material for these heat exchangers, the effective transfer of heat can be significantly increased while the size and weight of the heat exchanger is reduced.

A new, less time-consuming process for fabricating mesophase pitch-based graphitic foams without the traditional blowing and stabilization steps has been developed at Oak Ridge National Laboratory (ORNL) and is the focus of this research. Initially these foams possess a thermal conductivity of 106 W/m·K at a relatively low density of 0.54 g/cm^3. Potentially, the process will lead to a significant reduction in the cost of carbon-based thermal management materials (i.e., foam-reinforced composites and foam core sandwich structures).

Experimental

In this research, two 100% mesophase pitches were used to produce graphitic foam: Mitsubishi ARA24 naphthalene-based synthetic pitch (melting point of 237°C) and a proprietary mesophase pitch from Conoco Corporation labeled "Conoco Dry Mesophase" (melting point of 355°C). All foam samples were carbonized at 0.2°C/min to 1000°C and then graphitized at 10°C/min in argon to 2800°C with a 2-hour soak, at temperature.

In order to develop a fundamental understanding of the foam structure and graphitic morphology, and therefore develop an ability to tailor the thermal properties, samples were examined using a JOEL scanning electron microscope. Also, the thermal conductivity, κ, of the foam was determined with a xenon flash diffusivity technique. The thermal diffusivity, α, was first measured on samples of 12-mm diameter by 12-mm thickness on a custom-built machine in the High Temperature Materials Laboratory at ORNL. The sample density, ρ, and specific heat capacity, C_p, (assumed to be 713 J/Kg·°C) were then used to calculate the thermal conductivity with the following relation:

$$\kappa = \alpha \cdot \rho \cdot C_p.$$

Finally, the same foam samples used for thermal diffusivity were machined to cylinders of 12-mm diameter by 6-mm thickness for X-ray diffraction studies, giving an understanding of the relationship between processing conditions and the graphitic structure of the foam.

Several 38.1-mm-thick foam blocks were made from AR mesophase pitch with the standard ORNL process. Sandwich panels were constructed from 12.7-mm-thick, 152.4-mm-diameter foam core sections machined from the thick blocks. Both aluminum 3003-H14 and copper 110, 0.635-mm-thick, were used as face sheets. A thermally conductive film adhesive, T-gon 1/KA-08-128 (0.203 mm, 8 W/m·K), was used to bond the face sheets to the foam core with a cure at 0.241 MPa, 150°C for 30 minutes. Although a slightly higher pressure was recommended for curing the film adhesive, 0.241 MPa was found to be sufficient for bonding to the foam.

Flexural tests were conducted on 107-mm by 27.9-mm samples according to ASTM C393-94 for 4-point bending with two-point

loading and one-quarter span. This specimen geometry was chosen to produce core shear or bond failure. Compression testing was conducted at 5.08 mm/min for 19-mm-square samples.

The thermal conductivity of the laminated samples was determined by the same method as that used for the basic foam.

Results and Discussion

Figures 1 (a) and (b) are scanning electron micrographs of the pore structure of the Mitsubishi ARA24- and Conoco-derived foams, respectively, heat treated at 1000°C. The Conoco pitch yielded foams with marginally higher densities than foams produced with the ARA24 mesophase pitch. The ARA24 pitch-derived foams exhibited a larger mean pore size than the Conoco pitch-derived foams (275 μm vs. 60 μm). The higher melting temperature of the Conoco pitch yields higher viscosities during processing, and therefore smaller bubble sizes.

Both foams exhibit a spherical cell structure with open, interconnected pores (P in Figure 1) between most of the cells. It is evident from the images in Figure 1 that the graphitic structure in both foams is oriented parallel to the cell walls and highly aligned along the axis of the ligaments (L in Figure1).

It can be seen in the ARA24-derived foams that the graphitic structure is less aligned in the junctions between ligaments (J in Figure 1) and possesses more folded, mosaic texture. It is postulated that this arises from the lack of stresses at this location during forming.

Figure 2 is the X-ray diffraction spectra for both foams. The d_{002} spacing was calculated to be 0.3355 nm for the ARA24 foam and 0.3360 nm for the Conoco-derived foam. This is significantly better than in existing high-performance carbon fibers such as K1100 (0.3366) and vapor-grown carbon fibers (0.3366) and better than most synthetic carbons. The crystallite sizes (L_a and L_c) were similar to typical high-thermal-conductivity carbon fibers.

The thermal conductivity of the ARA24 foam graphitized at 10°C/min ranged from

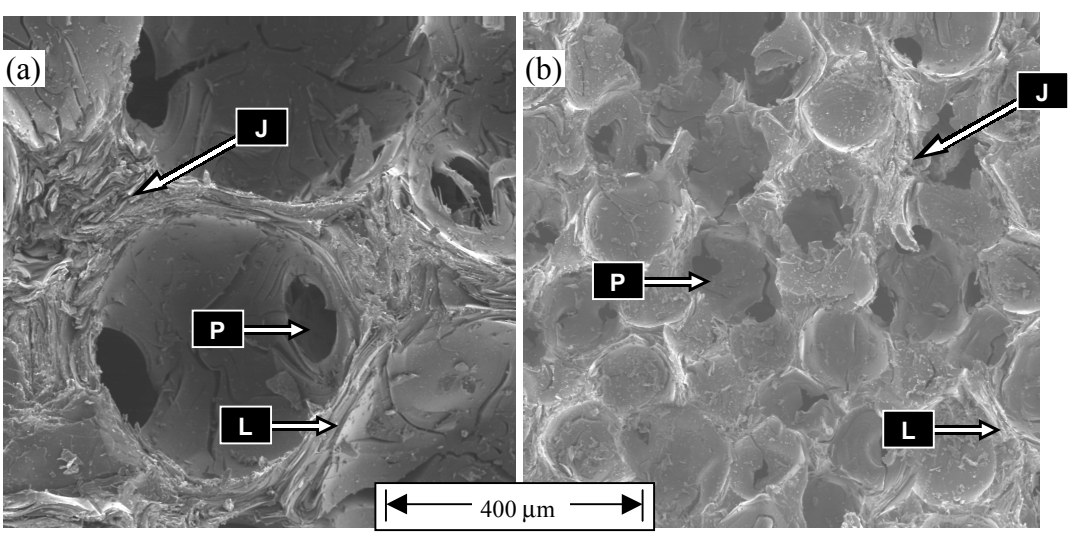

Figure 1. Structure of (a) Mitsubishi ARA and (b) Conoco Mesophase pitch-derived carbon foams carbonized at 1000°C.

50 to 150 W/m·K, and the Conoco derived foams exhibited thermal conductivities ranging from 40 to 135 W/m·K (Figure 3). These conductivities are remarkable for materials with such low densities, 0.27 to 0.57 g/cm^3 (density was varied by varying processing conditions).

Under close examination of the scanning electron microscope images in Figure 1, microcracks and delaminations of the graphite planes can be observed. These are most likely due to the thermal stresses induced during carbonization and graphitization as a result of the low thermal conductivity of the foam prior to graphitization. It was postulated that reducing the heating rates during this process would minimize thermal gradients, and thus minimize thermal stresses, resulting in fewer microcracks and delaminations. In fact, when the graphitization rate was slowed to 4°C/min, the thermal conductivity of the ARA24-derived foams increased significantly to nearly 190 W/m·K (Figure 3). This is significantly better than the targeted 50% increase in thermal conductivity.

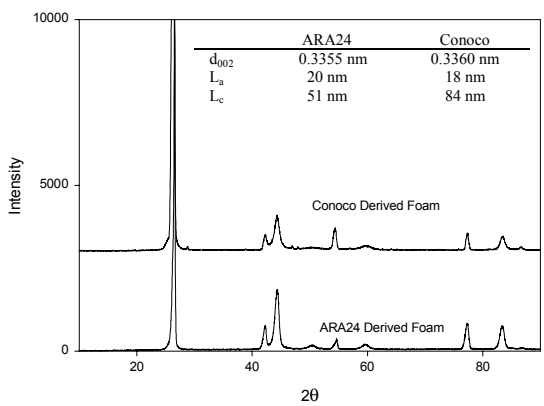

Figure 2. X-ray diffraction patterns of ARA24 and Conoco derived foams graphitized at 2800°C.

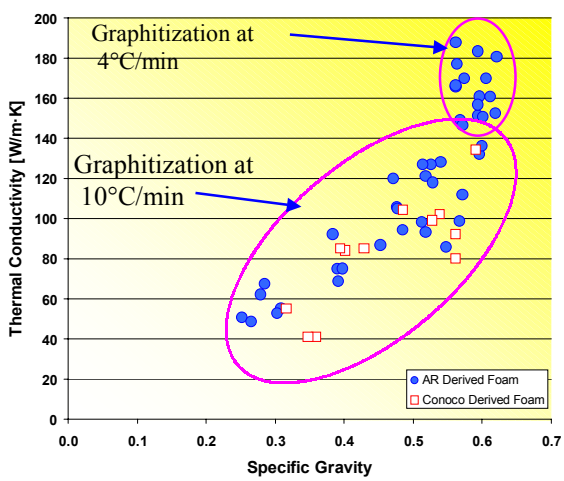

Figure 3. Thermal conductivity of ARA24 and Conoco derived foams as a function of density.

Four sandwich panels were fabricated for testing: two with aluminum face sheets and two with copper face sheets. The flexure specimens exhibited classic shear failure with only a slight delamination of the foam from the face sheet. The core shear stress ranged from 1.49 to 2.35 MPa, while the shear modulus ranged from 47.9 to 111 MPa. The values for panels with copper face sheets had a significantly higher core shear stress and core shear modulus that has not been explained.

A typical load-displacement curve for the compression tests shows that the foam core crushes with a fairly uniform load over a large displacement. The compression strength and modulus ranged from 1.2 to 2.5 MPa and 44 to 176 MPa, respectively.

The results of the thermal conductivity testing of the sandwich panels indicated that the sandwich specimens had a through-the-thickness thermal conductivity of between 50 and 65 W/m·K with little difference between the aluminum and the copper sandwich panels. Although the thermal conductivity was lower than that of the basic foam because of the relatively low-conductivity adhesive, the specific conductivity of the sandwich panels is comparable to that of aluminum.

The average adhesive thickness in the sandwich panels was between 0.127 and 0.203 mm. With a thermal conductivity of only 8 W/m·K, the interface was the limiting factor for the through-thickness conductivity. Methods to improve the through-thickness thermal conductivity include using a higher-conductivity adhesive and decreasing the adhesive thickness. Several additional sandwich panels have been successfully bonded with thinner bond lines of filled epoxies (approximately 0.0254 mm). Also, a brazing technique has been developed for bonding aluminum face sheets (thermal conductivity of the brazing material is approximately 45 W/m·K).

Applications

Since the foam is open cellular, it is a prime candidate for use as a porous media heat exchanger for a power electronics substrate. Currently, most substrates for high-power electronics include a water-cooled aluminum or copper plate mounted below the circuitry. It can be shown that the effective heat transfer coefficient can be raised from ~ 250 $W/m^2 \cdot K$ for current designs to over 10,000 $W/m^2 \cdot K$ for flow through a porous graphite foam. It was proposed that a once-through foam core/aluminum-plated substrate be fabricated to replace the current substrates (see Figure 4). The foam core thickness, geometry, channel patterns, foam cell size, and heat treatment temperature will be evaluated to give optimum heat removal at the lowest flow rate of cooling fluid.

In a separate test, heat transfer coefficients for a shell-and-tube heat exchanger with carbon foam as the core were measured as high as 11,000 $W/m^2 \cdot K$. This test validated the capability of the foams to remove large amounts of heat with cooling air instead of water.

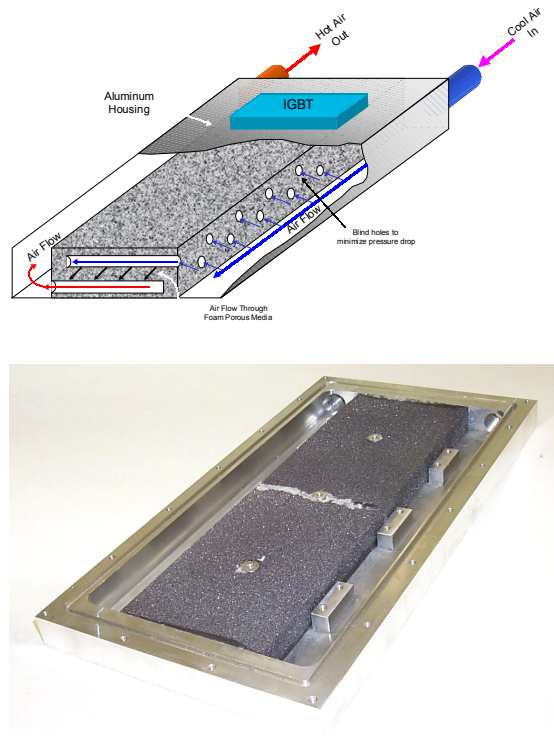

Figure 4. Schematic and photograph of design for foam-based heat exchanger substrate for power electronics cooling.

Furthermore, independent tests of the foam material at Florida International University have confirmed the dramatic improvement in heat transfer coefficients when the foam is used as a porous heat transfer medium. The major conclusion of this research is that natural convection is not enough to improve the heat transfer: the air must be forced through the foam to realize the full potential of the material.

A closed-form mathematical model was developed at the University of Tennessee to predict the thermal conductivity of the foam based on the structure and density. This model is being expanded to study the heat transfer characteristics of the foam under forced flow.

Extensive meetings are being conducted with DaimlerChrysler, Lockheed Martin,

Boeing, Modine, Peterbilt, and a NASCAR racing team to develop this material for radiator systems and other electronic cooling applications.

Conclusions

The highly aligned ligaments have similar structures to high-thermal-conductivity carbon fibers, such as K1100 and VGCF. In fact, the d-spacing was less than that of VGCF, which has exhibited thermal conductivities as high as 1950 W/m·K. These properties, combined with the continuous graphitic network, result in a specific thermal conductivity of up to 6 times greater than that of copper. Through this essential materials characterization, it was determined that slower heating rates during carbonization and graphitization would result in a dramatic improvement in thermal conductivity, nearly 75% better than the initial values. Hence, the main program objective was met.

Standard laminating techniques were shown to be viable for producing foam core sandwich panels. However, either thin bond lines or brazed interfaces were found necessary to preserve the high thermal conductivity. With further development, carbon foam can replace honeycomb in applications that require high thermal conductivity and low weight.

High heat-transfer coefficients have been measured, and heat exchangers have been designed and built with the knowledge learned in this program. In future research, extensive tests and redesigns will be conducted to build a proper heat exchanger substrate for power electronics cooling and other cooling applications for the Partnership for a New Generation of Vehicles.

The manufacture and properties of high-thermal-conductivity carbon foams have been reported. It was shown that pitch precursor characteristics will affect foam structure and properties such as bubble size, ligament structure, and thermal conductivity.

References/Publications

1. J. W. Klett, "Mesophase Pitch-based Carbon Foam: Effects of Precursor on Thermal Conductivity," The First Annual Carbon Foam Workshop, Kettering, Ohio, August 16–18, 1999.

2. J. W. Klett, "Mesophase Pitch-based Carbon Foam: Effects of Precursor on Thermal Conductivity," The 23rd Annual Conference on Ceramic, Metal, and Carbon Composites, Materials, and Structures, Cocoa Beach, Florida, January 1999.

3. J. W. Klett, "High Thermal Conductivity, Pitch-based Carbon Foam for Thermal Management Applications," The 22nd Annual Conference on Ceramic, Metal, and Carbon Composites, Materials, and Structures, Cocoa Beach, Florida, January 1998.

B. dc Buss Capacitors for PNGV Power Electronics

B.A. Tuttle, D. Dimos, G. Jamison, P.G. Clem, P. Yang, and D. Wheeler
MS 1405, Sandia National Laboratories
P.O. Box 5800, Albuquerque, NM 87185-1405
(505) 845-8026, fax: (505) 844-2974; e-mail: batuttl@sandia.gov

---

Objectives

- Develop a replacement technology for the presently used aluminum electrolytic dc buss capacitors for year 2004 new-generation vehicles.
- Develop a high-temperature polymer dielectric film technology that has dielectric properties technically superior to those of Al electrolytic dc buss capacitors and is of a comparable or smaller size.
- Develop a low-cost, multilayer ceramic technology that results in capacitors that are technically superior to presently used Al electrolytic capacitors.

Approach

- Contact automobile design and component engineers, dielectric powder and polymer film suppliers, and capacitor manufacturers to determine state-of-the-art capabilities and to define market enabling, technical goals.
- Synthesize conjugated polyaromatic chemical solution precursors that result in dielectric films with low dielectric loss and excellent high-temperature dielectric properties.
- Use a molecular engineering approach to create higher polarizabilities in polymer films, leading to higher dielectric constants, by substitution of side groups and bridging molecules.
- Fabricate, microstructurally analyze, and electrically characterize barium titanate and lead-based ceramics dielectrics in layers of suitable thickness for use in 2004 automobiles.

Accomplishments

- Determined critical issues for dc buss capacitors: (1) cost and hard breakdown for ceramic multilayers and (2) higher dielectric constants for polyfilm capacitors.
- Developed technologies for single-layer deposition thickness of 3 μm for polyfilm capacitors and layer thickness ranging from 20 μm to 50 μm for ceramic capacitors using computer-controlled micro-pen and tape cast technologies (these would be suitable for 600-V dc buss capacitor operation).
- Designed and fabricated polyfilm dielectrics with dielectric constants of 4 and dielectric loss less than 0.003, which exceeded the properties of state-of-the-art polyphenylene sulfide.

- Fabricated ceramic dielectrics with high permittivity that met or exceeded manufacturer's specifications and that were compatible with low-cost electrode approaches (ultralow fire and base metal electrode). Performed a trade-off study of performance versus electrode cost for low-fire barium titanate dielectrics.

Future Directions

- Enhance dielectric constant of polymer film dielectrics to greater than 6 and keep dissipation factor below 0.01. Commercial manufacturers have stated that these properties would spur commercial development.
- Develop low-cost electrode, ceramic dielectric capacitor technology that can withstand high electrical breakdown fields.
- Fabricate multilayer polyfilm and ceramic dielectrics that meet PNGV electric field operation criteria to reduce size of units.

Introduction

Sandia National Laboratories (SNL) has actively interacted with a number of representatives from the automobile industry to obtain their perspective on what is needed for 2004 automobiles. These representatives included Gary Crosbie and Paul Crosby (Ford), Balarama Murty and Jim Nagashima (General Motors), and Alvin White (Daimler Chrysler). Sandia has also actively interacted with a variety of capacitor manufacturers and dielectric powder suppliers. These suppliers included AVX, Murata, Kemet, Degussa, TAM, Ferro, TPL Inc., TRS Ceramics, Materials Research Associates, Tokay, and TPC Ligne Puissance.

These interactions led us to the conclusion that the two most viable replacement technologies for the electrolytic dc buss capacitors by 2004 were multilayer ceramic and multilayer polymer film capacitors. Although the greatest concern regarding the multilayer ceramic capacitors (shown in Figure 1) was the cost, reducing the size of the polymer capacitors was most often cited by automobile design engineers as a needed technology-enabling breakthrough. Thus, Sandia is targeting technical solutions that will reduce the cost of ceramic multilayer capacitors and that will increase the dielectric constant of the polyfilm dielectrics, thereby leading to smaller capacitors. The industry would like to have higher field operation for low-cost multilayer ceramic technologies, such as base metal (BME) and ultra-low-fire (ULF) dielectrics. A dielectric constant of 1000 at a dc field of 200 kV/cm has been stated as a goal for power electronics by AVX and the Center for Dielectric Studies at Penn State. Both the BME and ULF technologies substantially reduce the cost of multilayer ceramic capacitors by permitting the use of lower-cost Ni or Ag electrodes instead of high-Pd-content electrodes. The electrodes comprise roughly 95% of the total cost of a

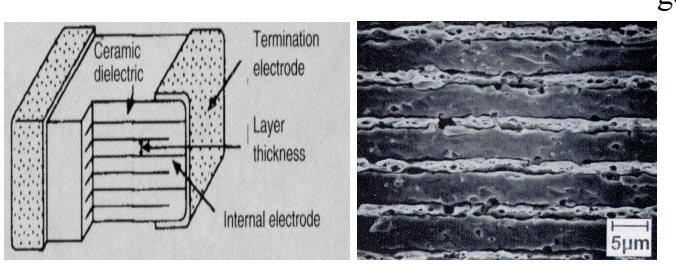

Figure 1. Multilayer ceramic capacitor schematic and micrograph of cross-sectional view.

ceramic multilayer capacitor. Other considerations expressed by the auto manufacturers were cost, hard breakdown behavior in ceramics, and the high-temperature performance of polymer film capacitors. Inverter designs and operating conditions for dc buss capacitors vary from manufacturer to manufacturer. We presented our assumption of 450-volt dc operation with 125-volt spike voltages for a nominal 500 µF dc buss capacitor, which was well received at the DOE Merit Review Meeting.

While size and outstanding temperature performance are advantages for the ceramic technologies, soft breakdown behavior and lower cost are assets for polymer film capacitors.

Polymer Film Dielectric Development

SNL polymer film dielectric development has been based on the request from manufacturers that the new polyfilm dielectrics have voltage and temperature stability that is equivalent to present polyphenylene sulfide (PPS) technology. Thus, a structural family of polymer dielectrics has been designed and synthesized to meet two of the most stringent PNGV requirements: (1) low dielectric loss and (2) extremely good temperature stability. Figure 3 shows a schematic diagram of Sandia's conjugated, polyaromatic-based structure and indicates the large number of molecular modifications to this structure that are possible. Our present effort emphasizes molecular

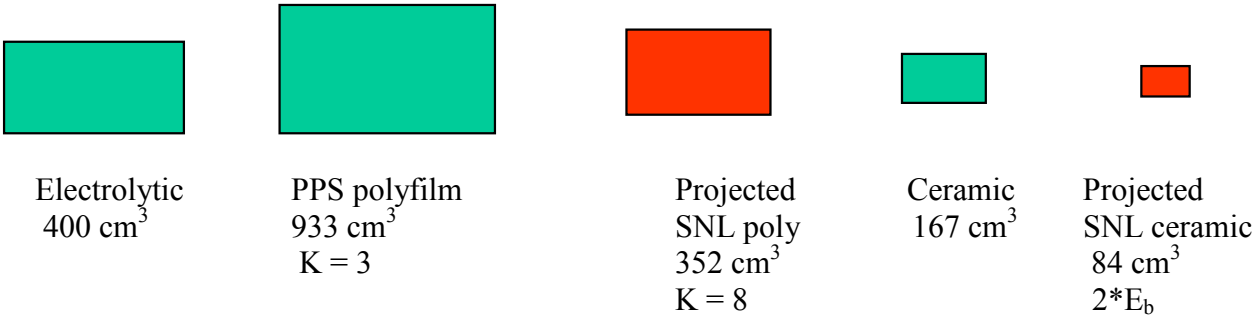

Figure 2. Size diagram of 500 µF dc buss capacitors of different technologies.

Based on these criteria, an individual dielectric layer thickness of approximately 3 µm for polyfilm and 40 µm for ceramic capacitors is projected. Operating field strengths of 2 MV/cm and 150 kV/cm are projected for polyfilm and ceramic dielectric capacitors, respectively. Based on these assumptions and on measurement of presently available commercial capacitors, size comparisons of 500 µF dc Buss capacitors for different technologies were obtained (Figure 2).

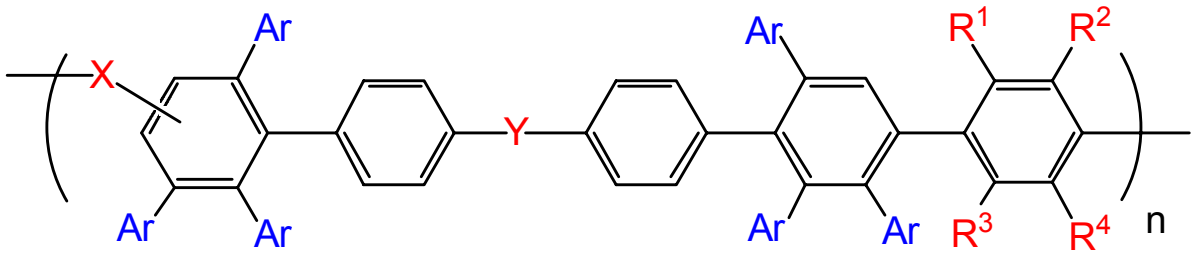

Figure 3. Schematic diagram of SNL conjugated polyaromatic film base structure.

engineering of higher-polarizability structures that will enhance dielectric constants, yet retain acceptable dielectric loss characteristics. A patent disclosure has been issued covering the design and synthesis techniques for this polymeric family. Three initial molecular modifications to the base structure were made: (1) propyl bridge substitution, (2) sulfur bridge substitution and (3) replacement of R side groups with high-electronegativity fluorine ions to enhance polarizability.

The initial dielectric properties of a series of films of approximately 0.4 µm thickness are shown in Table 1. The industry standard high-temperature performance polyfilm dielectric, PPS, has a dielectric constant of 3, a dissipation factor of 0.003 and a breakdown field of 2.2 MV/cm at 25°C. We have increased the dielectric constant to approximately 4, while maintaining similar loss and breakdown field characteristics. Breakdown field is very much a function of the processing environment and, in production-type environments, it is anticipated that the breakdown field will be substantially enhanced. An example is shown in the bottom row of the table for polyvinylidene fluoride (PVF2) films that were processed using a chemical vapor deposition technique at Sandia. Breakdown fields of 5.5 MV/cm were obtained for these films and indicate the potential 6-fold increase in energy density possible for the next generation of chemically deposited polyfilms. Although the fluorine substitutions did not yield the hoped-for enhancement in dielectric constant, numerous other promising molecularly modified polymer dielectrics will be synthesized in FY 2000.

Table 1. SNL polyfilm dielectric properties for initial molecular modifications.

Sample description	Dielectric constant	Dissipation factor	Breakdown field (MV/cm)
Propyl bridge	4.0	.003	1.9
Sulfur bridge	3.8	.002	1.7
Fluorine side group substitution	3.9	.001	1.8
PVF2 vapor deposited	4.1	.005	5.5

Ceramic Dielectric Layer Fabrication and Characterization

Ceramic dielectric layers were fabricated using two different techniques: (1) conventional tape casting and (2) computer-controlled micropen technology. For the micropen deposition, a ceramic slurry in the form of a 30-micron-diameter tube is deposited onto the desired substrate (Figure 4). We have demonstrated high-quality dielectric layers of thickness as low as 20 microns using this technique. Both chemically prepared barium titanate–based dielectric powders from Degussa and conventional state-of-the-art mixed oxide powders from TAM have been fabricated into dielectric layers using this technique. Further, an initial study to determine dielectric properties as a function of firing temperature has been completed. Dielectric layers processed at 850°C had lower dielectric constants, but they could be processed using inexpensive electrodes with

high Ag content. Layers processed at higher temperatures had higher dielectric constants but required more expensive electrodes with high Pd content for compatibility. The layers processed at high temperature (1320°C) had dielectric constants of 3000, while films processed at lower temperature (900°C) had dielectric constants of 1000. Studies of breakdown strength versus temperature are in progress for the layers produced by the different processes.

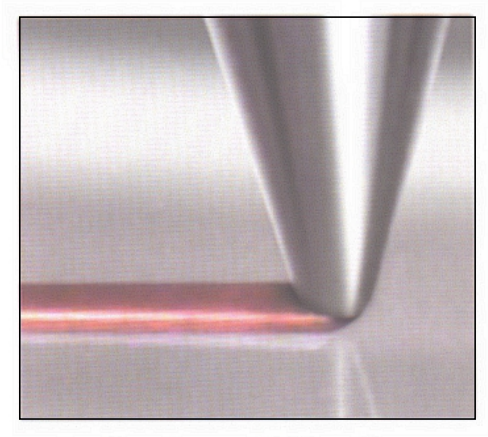

Figure 4. Micropen CAD/CAM Direct Write (30 µm to 500 µm lines).

In addition to micropen deposition, conventional tape casting processes were developed. Presently, a 40-µm-per-layer process has been optimized for high-altitude depositions and has resulted in dielectric layers with properties comparable to those specified by commercial manufacturers in state-of-the-art multilayer ceramic fabrication facilities. Table 2 shows the dielectric constants obtained from chem-prep (Degussa) and mixed oxide (TAM) barium titanate–based powders using different deposition methods.

Summary

Critical economic and technical issues for improvements of dc buss capacitors for new-generation vehicles were determined through discussions and visitations with automobile design engineers and capacitor manufacturers. We have been able to fabricate new polymer film dielectrics with a 33% increase in dielectric constant compared with industry standards, while maintaining voltage and dielectric loss stability. The goal in FY 1999 is to increase the dielectric constant of the Sandia-designed polyfilms by 100% while keeping losses below 1%. Thus, the polymer film task is at the stage where the appropriate foundation or backbone chemistry development is completed. In the future, mole-cular modifications to this backbone chemistry should lead to substantial enhancements in dielectric constant.

Two different techniques were developed to fabricate ceramic layers of a thickness suitable for high-voltage dc buss capacitor applications. Dielectric properties of both tape-cast and micropen-deposited layers were equivalent to state-of-the-art commercial multilayer dielectrics. Thus, the foundation has been formed for the evaluation and enhancement of both ULF and BME ceramic dielectrics via proper selection of dopants and low-level additives in FY 2000.

Table 2. Dielectric properties of micropen and tape cast layers

Sample	K, commercial multilayer	K, SNL micropen	K, SNL tape cast	K, SNL bulk ceramic
Degussa, X76 CP, 1310°C	3200	3200	3400	2595
TAM X7R 262L, 1140°C	2242	2240	2056	2062

C. Mechanical Reliability of Electronic Ceramics and Electronic Ceramic Devices

A. A. Wereszczak and K. Breder
Mechanical Characterization and Analysis Group (MCAG)
Oak Ridge National Laboratory, P.O. Box 2008, MS 6069, Bldg. 4515
Oak Ridge, TN 37831-6069
(865) 574-7601; fax: (865) 574-6098; e-mail: wereszczakaa@ornl.gov

---

Objectives

- Develop testing algorithms that can be used to assess electronic ceramic (EC) and electronic ceramic device (ECD) mechanical reliability.
- Mechanically characterize EC and ECD alternatives that are less expensive and that can be used to promote device miniaturization.

Approach

- Utilize micromechanical testing and ceramic-specific-characterization testing facilities to measure in situ mechanical properties of ECs in the ECDs.
- Characterize presently used and developmental EC and ECDs supplied from their manufacturers or their end-users.
- Use already-developed ceramic component prediction codes (whose development was funded by the Office of Transportation Technologies/Ceramic Technology Project for structural ceramics) and their statistical analysis capabilities in analyzing the mechanical strength and fatigue of ECs and ECDs.
- Provide results and insights back to manufacturers that will result in the improved reliability of ECs and ECDs.

Accomplishments

- A mechanical properties microprobe (MPM) was used to characterize $BaTiO_3$ dielectrics in snubber multilayer capacitors (MLCs). It was found that mechanical performance (e.g., fracture toughness, strength) of ceramic dielectrics can be significantly different in equivalent snubber MLCs.
- Strength and fatigue of two alumina substrates and an aluminum nitride substrate were characterized and mechanical design data were generated for use with ECDs.
- The fatigue and strength testing of candidate tape-cast aluminas for automotive gas exhaust sensors was initiated in collaboration with Motorola.

Future Direction

- Acquire commercially available dc buss MLCs and measure the in situ mechanical performance of their dielectric ceramics. Collaborate with Sandia National Laboratories

in the characterization of the dielectric ceramic in their developmental dc buss MLCs for automotive power electronics building blocks.

- Characterize less expensive Ni-electrode snubber MLCs.
- Study the utility of non-destructively measuring residual stresses in MLCs with piezospectroscopy and non-destructively identifying damaged MLCs with resonant ultrasound spectroscopy.

Introduction

A lack of mechanical reliability of ECs in ECDs can often limit the reliability of their electronic function. Three classes of ECs or ECDs that this project examined in FY 1999 were multilayer capacitors (MLCs), EC substrates, and oxide ceramics for automotive exhaust gas sensors; the service life of all three can in fact be limited by their mechanical reliability. The application of ceramic life prediction codes (developed for structural ceramic component design in high-temperature gas turbine engines) is used in concert with the mechanical testing analyses of the ECs because they portray the probabilistic strength and fatigue properties of ECs in an appropriate (but underutilized) manner.

One MLC manufacturer states that 40–50% of its capacitor failures are mechanically induced. Although its MLC failure rate is only on the order of 1 part per million, since the company manufactures 30–40 million capacitors a day, this failure rate is actually significant. Therefore, the company (and its customers) have a vested interest in improving MLC mechanical reliability. A goal of this project is to help MLC manufacturers improve this reliability.

Measuring the mechanical performance of dielectric ceramics in MLCs is not trivial because of their very small size. An MPM in the Mechanical Characterization and Analysis Group was used to measure in situ fracture toughness of the dielectric ceramic in equivalent, commercially available, snubber MLCs. Although the MLCs had equivalent capacitances, the fracture toughnesses of their dielectrics were statistically different, as shown in Figure 1. Fracture toughness is an indicator of mechanical robustness, and an end-user of these three MLCs (an automobile manufacturer) stated that it had experienced increasing reliability with the MLCs in this examination with higher fracture toughnesses. These results suggest that

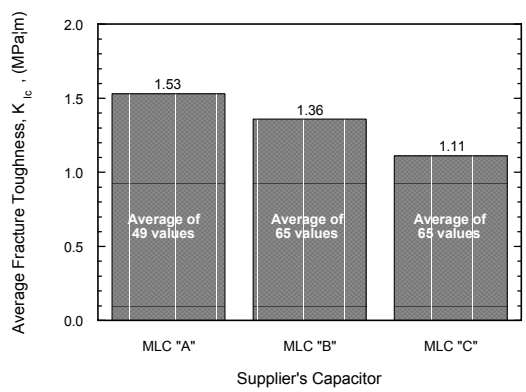

Figure 1. The fracture toughness of the dielectric ceramic in equivalent snubber multilayer capacitors was different. The difference was statistically significant.

MLCs that have a dielectric ceramic with maximum toughness will offer better mechanical reliability.

Additional techniques to assess mechanical robustness of MLCs were also examined and developed. Image analysis was coupled with fracture mechanics and Weibull theory to

"calculate" the strength distribution of dielectric ceramics in MLCs. This technique, along with fracture toughness measurement, helps portray the whole mechanical performance of dielectric ceramics.

The strength and fatigue of three commercially available ceramic substrates were characterized. Two of the substrates were aluminas (a tape-cast and a roll-compacted material), and the third material was an aluminum nitride (AlN). The tape-cast alumina (Al_2O_3) was stronger and more fatigue-resistant than the roll-compacted Al_2O_3 (commonly used in ECDs), but it was more costly. The AlN was not as strong as the tape cast Al_2O_3, but it was stronger than the roll-compacted Al_2O_3 and much more fatigue-resistant, as compared in Figure 2 (and was the most expensive of the three). The results from this study will help end-users of ceramic substrates appropriately design with and choose them.

Motorola is developing an automotive exhaust gas sensor; this project is assisting its development. The sensor is a multilayer design and will be using Al_2O_3 as a matrix; however, an alumina with optimum strength and fatigue (which is also inexpensive) has not yet been identified. The mechanical testing of three Al_2O_3s was initiated during FY 1999 to measure their strength as a function of temperature, as well as their fatigue performance. The highest purity of Al_2O_3 examined had the lowest strength at room temperature, while the least pure Al_2O_3 had the highest strength at room temperature, as shown in Figure 3. However, recent results show that the lowest-purity Al_2O_3 has the worst fatigue resistance of the three and was no longer the strongest Al_2O_3 of the three at 1000°C (an expected service temperature of the sensor).

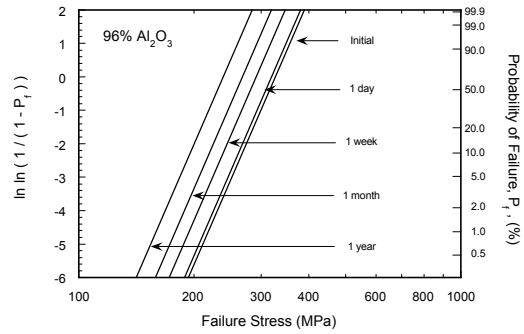

Figure 2a

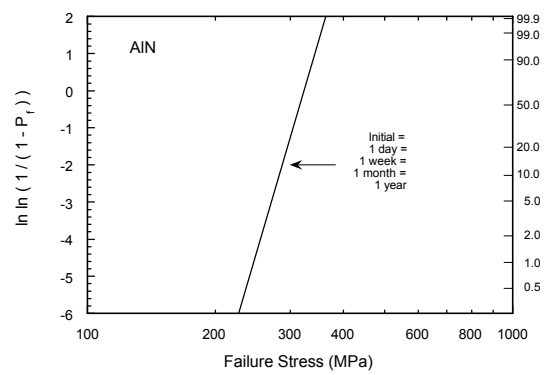

Figure 2b

Figures 2 a and b. A 96% alumina material (2A) was found to be susceptible to fatigue at 20°C, while AlN (2B) was not. The alumina tested is a commonly used ceramic substrate; the AlN substrate is more costly but has better thermal conductivity and a thermal expansion similar to that of silicon.

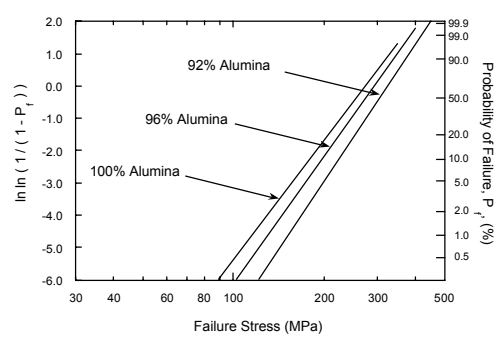

Figure 3. The 20°C strength of 92% alumina was the highest, followed in turn by the 96% and 100% aluminas. All aluminas are candidates for Motorola's automotive exhaust gas sensor.

Summary

The present project's FY 1999 mechanical testing results, characterization, and analyses of all three classes of these ECs and ECDs will help manufacturers (1) identify ECs that will prolong the service life of ECDs and (2) design their ECDs so that deleterious stresses are not imposed within them during their manufacture or service. Fracture toughness and strength results and analyses of dielectric ceramics in MLCs are being used by MLC manufacturers to improve the overall mechanical robustness of their MLCs. Strength and fatigue results and analyses of Al_2O_3 and AlN ceramics will help ECD manufacturers choose an appropriate ceramic substrate (and design) for their ECD that promotes longer service life. Finally, high-temperature strength and fatigue results and analyses of candidate Al_2O_3s will help this original equipment manufacturer identify the optimum and best-performing Al_2O_3 for their developmental automotive exhaust sensor.

References/Publications

1. A. A. Wereszczak, T. P. Kirkland, and K. Breder, "Biaxial Strength, Strength-Size-Scaling, and Fatigue Resistance of Alumina and Aluminum Nitride Substrates," in review, *International Journal of Microcircuits and Electronic Packaging*, 1999.

2. K. Breder, A. A. Wereszczak, L. Riester, and T. P. Kirkland, "Determination of Strength for Reliability Analysis of Multilayer Ceramic Capacitors," in press, *Ceramic Engineering and Science Proceedings*, Vol. 20, 1999.

3. A. A. Wereszczak, A. S. Barnes, and K. Breder, "Probabilistic Strength of {111} n-Type Silicon," in review, *International Journal of Microcircuits and Electronic Packaging*, 1999.

4. A. A. Wereszczak, R. S. Scheidt, and K. Breder, "Probabilistic Thermal Shock Strength Testing Using Infrared Imaging," in review, *Journal of the American Ceramic Society*, 1999.

5. A. A. Wereszczak, K. Breder, M. K. Ferber, R. J. Bridge, L. Riester, and T. P. Kirkland, "Failure Probability Prediction of Dielectric Ceramics in Multilayer Capacitors," pp. 73–83 in *Multilayer Electronic Ceramic Devices, Ceramic Transactions, V97*, American Ceramic Society, 1999.

D. Low-Cost, High-Energy-Product Permanent Magnets

Tom M. Mulcahy and John R. Hull
Argonne National Laboratory, Energy Technology-335
Argonne, IL 60439
(630) 252-6145; fax: (630) 252-5568; e-mail: mulcahy@anl.gov

Andrew E. Payzant
Oak Ridge National Laboratory, MS-6064, P. O. Box 2008
Oak Ridge, TN 37831-6064
(865) 574-6538, fax: (865) 574-4913; e-mail: payzanta@ornl.gov

---

Objectives

- Develop a low-cost process to fabricate NdFeB permanent magnets with up to 25% higher strengths. The higher-strength magnets will replace ones made by traditional powder metallurgy and enable significant size and weight reductions of traction motors for hybrid vehicles.
- Utilize high-strength superconducting magnets to improve the magnetic alignment of grains prior to pressing and sintering, therefore producing higher-strength magnets.
- Collaborate with magnet manufacturers, who will provide powder, sinter the green compacts, and perform characterizations of the engineering magnetic properties.

Approach

- Develop facilities to align magnetic domains of NeFeB powders within a high-strength magnetic field, created by a superconducting magnet, during forming operations.
- Characterize, compare, and correlate engineering and microscopic magnetic properties of magnets processed under varying conditions, including some in current production.
- Utilize a reciprocating feed to automate insertion of loose and compacted magnet powder into and out of the steady field of a superconducting solenoid.

Accomplishments

- Completed design of an axial-die press for making 1- to 2-cm-diameter permanent magnets in a batch mode.
- Fabricated and assembled an Axial-Die Press facility at Argonne National Laboratory that includes a 9-Tesla superconducting magnet.
- Characterized magnetic properties of permanent magnets provided by manufacturers.

Future Directions

- Optimize fabrication processing and powders from different industrial partners using axial-die and isostatic pressing in batch mode operations.
- Design, fabricate, and operate a reciprocating press in a continuous mode to demonstrate the feasibility of competitive factory operation.
- Optimize fabrication processing and powders from different industrial partners, using transverse-die pressing and a reciprocating press.
- Provide design rules for the fabrication of permanent magnets, including knowledge for scale-up to larger size magnets at commercial rates of production.

Introduction

A Cryomagnetics, Inc., superconducting solenoid has been specified and purchased, after consultation with permanent magnet manufacturers. The magnitude of the steady field in the bore of the solenoid can be continuously varied up to 9 Tesla. Magnet powder can be aligned in a field that is uniform within 5%, over a volume that is large enough to axial-die press 1- to 2-cm-diameter cylindrical magnets that have similar lengths. Alternatively, a 2.5-cm-diameter by 12.5-cm-long volume of powder, contained in a rubber mold, can be aligned for subsequent isostatic pressing.

The axial-die and punch set shown in Figure 1 was designed in consultation with the permanent-magnet manufacturer UGIMAG, Inc. and the tooling fabricator Bronson and Bratton, Inc. The set was made using very low-magnetic-permeability material (<1.002), which will not affect significantly the uniformity of the superconducting solenoid's magnetic field or the alignment of the magnet powder. However, self-demagnetization fields are inherent in short cylinders of magnet powder and can affect the applied field uniformity and grain alignment of permanent magnets. This happens in current production, where, typically, electromagnets provide alignment

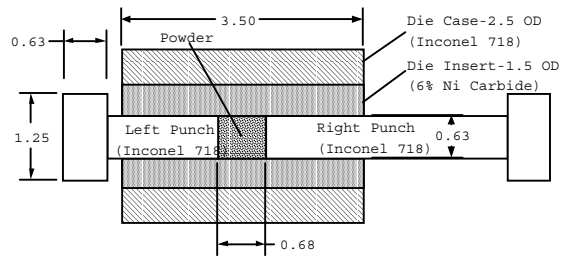

Figure 1. Axial-die and punch set for 5/8 in. magnet; powder shown is compacted.

fields of less than 2 Tesla, which approaches the saturation limit of the steel present in commercial presses. Vector field electromagnetic code calculations were made that showed demagnetization effects were still pronounced up to applied alignment fields of 7 Tesla, which can be exceeded with the superconducting solenoid purchased.

An unorthodox press-in-tube method for axial-die pressing in a batch mode was devised and built by Ability Engineering Technology, Inc., which met the magnetic, geometric and program cost constraints associated with using superconducting solenoids (see Figure 2). The press tube and ram are made from very low-magnetic-permeability materials (< 1.002). The hydraulic cylinder was custom made, by Atlas Cylinders, Inc., from stainless steel with a low permeability (< 1.010). The length of the press tube was made sufficient

to locate the more magnetic hydraulic cylinder in the far field of the solenoid, where the magnetic-field gradient is weak, and to access the solenoid, which is thermally shielded deep within its helium Dewar. Electromagnetic code calculations were made to determine the far magnetic field and maintain minimal magnetic forces between the solenoid and the axial-die press.

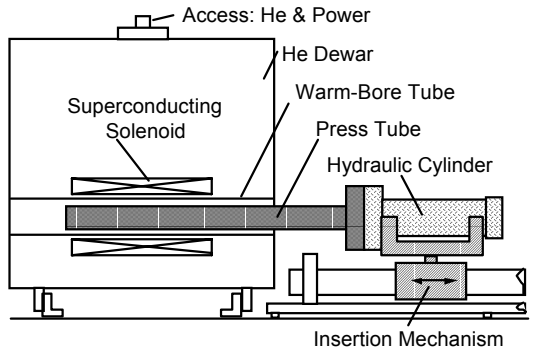

Figure 2 (a). Axial-die press in the solenoid.

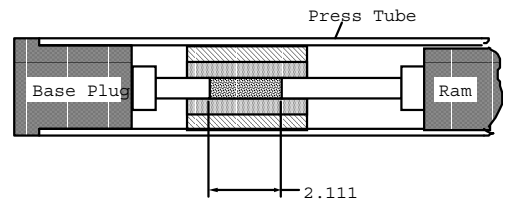

2 (b). Press-tube interior; no compaction.

The press insertion mechanism enables complete and controlled removal of a green compact from the Dewar's warm-bore tube, while the superconducting solenoid is operating and the hydraulic cylinder is activated. This feature allows the experimental determination of extraction and insertion forces, which will be used to calibrate electromagnetic code models already developed. Understanding the forces and their minimization is key to the design of a reciprocating press. Also, the mechanism allows rotation of the end of the press tube into the solenoid's weak fields (< 250 Gauss) for removal of the green compacts.

The capability to move the axial-die press into the far field of the solenoid allows exploration of another processing method. In isostatic pressing, the powder is aligned separate from the pressing operation. Argonne National Laboratory maintains an isostatic press that exceeds the capabilities of magnet manufacturers. Discussions with manufacturers and a review the journal and patent literature indicates that the greater alignment fields of superconducting solenoids will be less effective in energy-product improvement, because self-demagnetization effects are much less for the long, powder-filled cylindrical rubber molds used in isostatic pressing. Also, because the commercial electromagnetic alignment solenoids are separatefrom the press and can be isolated from ferromagnetic material, they can provide multiple, higher-field alignment pulses (< 6 Tesla) to the powder. In addition, enhancements can be achieved by mechanical manipulation of the rubber molds. Currently, isostatic pressing is claimed to produce permanent magnets that are within 5–10% of having optimal alignment and magnetic properties. However, the alignment of powder has never been attempted in the steady, high fields available with the superconducting solenoid. Other processing improvements may be possible, such as an ability to align a more economical powder that has a wider particle-size distribution. The magnet

producer CRUMAX will participate in identifying any benefits.

The magnet manufacturers provided characterized permanent magnets: transverse-die pressed 26-mm cubes and two sets of isostatically pressed cylindrical magnets with diameters of 14–15 mm. The energy products of the cubes were 41 MGOe. One set of cylinders had a 45-MGOe energy product, which was significantly different from the other's 35 MGOe. The two sets were made using different processes. At Argonne, the remnant induction of each magnet was measured by rotating it in a Helmholtz coil. The manufacturer's values, which ranged from 1.2 to 1.35 Tesla, were confirmed.

At Oak Ridge, an examination of microstructure and preferred orientation revealed clear differences between samples. Electron microprobe analysis of each manufacturer's products showed the composition of their grain boundary phases to be slightly different; however, the primary phase was chemically identical. X-ray diffraction pole figures were used to characterize the texture on the face normal to the magnetization axis.

Data were collected at 5-degree tilt and rotation increments using Cu k-alpha X-ray radiation with 1-mm diameter incident beam collimation. The strongest preferred orientation was observed for one of the isostatically pressed cylindrical magnets, as shown in Figure 3, whereas the other cylindrical magnet had the weakest texture, as shown in Figure 4. Both of these showed a fiber texture with cylindrical symmetry.

The cube samples were strongly textured, only slightly less so than the strongest cylindrical sample, and both were nearly identical. Their texture was not perfectly cylindrical, as shown in Figure 5. This was not unexpected for transverse-die pressing, where compaction is unidirectional and normal to the direction of magnetization.

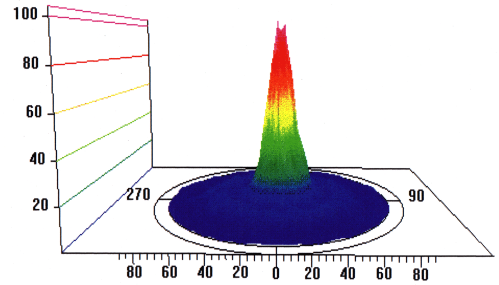

Figure 3. Oblique view of 006 pole figure of the cylindrical sample showing axial symmetry characteristic of strong "fiber" texture. Peak height = 105 cps.

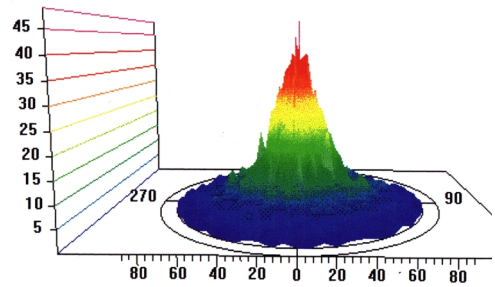

Figure 4. Oblique view of 006 pole figure for the cylindrical sample showing axial symmetry characteristic of moderate "fiber" texture. Peak height = 49 cps.

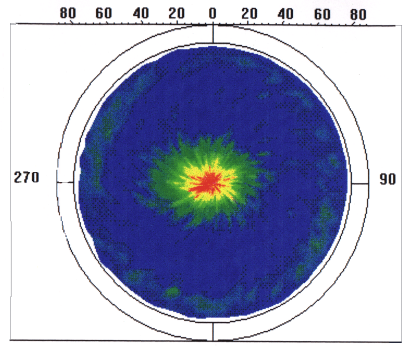

Figure 5. Top view of 006 pole figure for a cube sample, showing slightly distorted cylindrical symmetry. Peak height = 100 cps.

The correlation of these texture measurements with the energy product and methods of pressing is a clear demonstration of the importance of improved grain alignment and the utility of microstructure analysis, in particular, X-ray diffraction analysis, in quantifying subtle variations in texture produced by different methods of processing.

E. Lead-Free Solders for Automotive Electronics

M. L. Santella, R. J. Barkman, and M. J. Gardner
Oak Ridge National Laboratory, Metals & Ceramics Division
Oak Ridge, TN 37830-6096
(865) 574-4805, fax: (865) 574-4928; email: santellaml@ornl.gov

---

Objective

- Support development of lead-free, high-temperature "engineered" solder alloys for automotive electronics applications such as power electronics devices by systematically determining the effects of alloying on the properties, soldering characteristics, and microstructure of Sn alloys.

Approach

- A series of binary alloys are formulated to determine the effects of individual alloying elements on mechanical properties, the wetting behavior on copper, and melting characteristics.
- A micromechanical testing technique is being used to determine the mechanical properties of solder alloys in situ in solder joints.

Accomplishment

- The feasibility of using automated ball indentation testing to measure the tensile properties of solder bumps was demonstrated. This indicates that measurement of solder joint properties is also feasible.

Future Direction

- The effects of major alloying elements such as Bi, Cu, In, Sb, and Zn on tensile properties, wetting behavior, microstructure, and melting characteristics will be determined.
- Alloying elements will be identified that improve the ductility of Sn, as this is expected to favorably impact solder joint reliability and the resistance to fillet lifting in through-hole connections.
- Some effort will be directed toward perfecting micromechanical testing of solder joints.

Introduction

Lead is recognized as a significant threat to both the environment and public health, and pending legislation could result in the banning of lead from a wide variety of products, including electronics. The overall objective of this project is to develop lead-free, high-temperature "engineered" solder alloys that will increase the operating temperature of automotive electronic packages from 120°C to 180°C. The initial emphasis is on studying the properties and

characteristics of tin alloys because they are most likely to form the basis of high-temperature soldering alloys such as eutectic Sn-Ag.

During FY 1999, significant progress was made toward determining the feasibility of using automated ball indentation (ABI) testing to measure the tensile properties and strain rate sensitivity of solder joints. Because of its importance to reliability, the mechanical behavior of existing and newly developed solder alloys is a key concern in the design and engineering of advanced electronic components. Standard tensile testing is commonly used to determine alloy strength and ductility properties, but there is concern that tensile testing may not provide an accurate indication of actual solder joint performance. Part of the basis for this concern is that the thermal processing conditions experienced during joint manufacturing may not be accurately reproduced in bulk alloy tensile specimens. This means that the mass transport conditions and chemical reactions that occur in joints and that will influence their properties are unlikely to be reflected in standard test data. The ABI testing was viewed as a novel way to measure the mechanical properties of actual joints.

Subsized tensile specimens were made from 1.5-mm-thick rolled sheets of pure Sn, Sn–3.5Ag, Sn-37Pb, and Pb–5Sn (nominal compositions wt %). The Pb alloys were included as standard reference alloys. These specimens were tested at room temperature to determine baseline tensile properties.

Subsequently, ABI tests were performed on the shoulder areas of the same specimens as indicated schematically in Figure 1.

Images of the ABI indentations taken in a scanning electron microscope (SEM) are

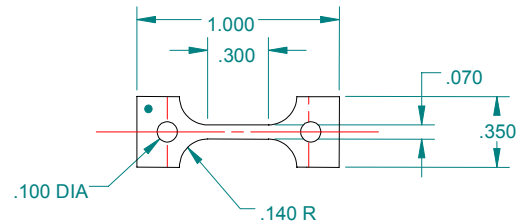

Figure 1. Schematic of solder alloy tensile specimen showing relative size of ABI indent on specimen shoulder (dot on upper left corner).

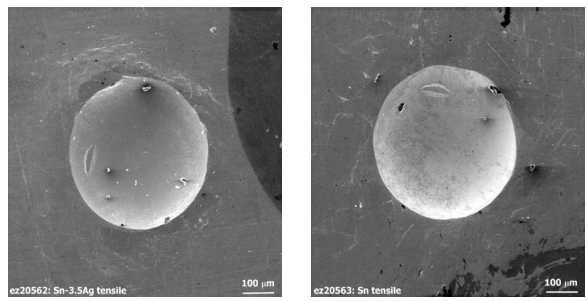

Figure 2. ABI indentations on tensile specimens of pure Sn (right) and Sn–3.5 Ag solder alloy (left).

shown in Figure 2. The indentations are circular, as required for data analysis, and the plastic zones surrounding them are evident. During the tests, both the load and indentation depth are very accurately measured and used to determine a plastic flow curve where the true strain, ε_p, and the true stress, σ_p, are given by

$$\varepsilon_p = 0.2\frac{d_p}{D} \qquad \sigma_p = \frac{4P}{\pi d_p^{\,2}\delta} \quad .$$

The quantity d_p is geometrically related to indentation depth, D is the indenter diameter, P is the applied load, and δ is a constant determined from the test data. The yield strength is also determined from the ABI test using a separate calculation.

Overall, however, there was good agreement between the two data sets. The ABI test was originally developed for use on steels, for which it provides very accurate measurements of tensile properties. This

experiment established that the ABI test was also capable of determining tensile properties of solder alloys with reasonable accuracy (see Figure 3).

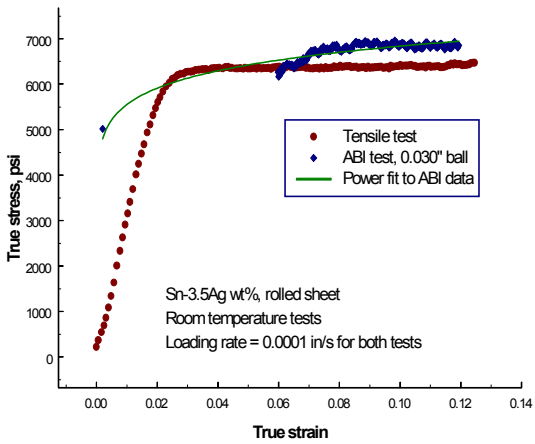

Figure 3. Comparison of tensile and ABI test data from bulk specimen of Sn–3.5Ag solder alloy.

Next, small FR4 printed-circuit test boards were obtained that contained arrays of solder bumps made with Sn–3.5Ag solder alloy. The solder bumps had nominal dimensions of 2.5 mm length by 0.8 mm width by 0.30–0.50 mm thickness. The ABI test requires a flat surface for accurate measurements, so flat spots were made on the solder bumps using a polishing technique.

The sizes and shapes of the solder bumps before and after preparation of flat spots are shown in Figure 4.

The appearance of several solder bumps after ABI testing is presented in Figure 5. The indentations on the bumps at the top left position and bottom right position of Figure 5 show uniform circular impressions that are consistent with obtaining acceptable data. The indentation on the lower left has an irregularity on its diameter that was produced by a defect in the solder bump. The impression on the upper right is actually a porosity defect in the solder bump rather than an indentation from testing. The existence of defects was unexpected, and they only became apparent in the solder bumps as the ABI tests were being conducted. Figure 5 further illustrates the accuracy with which the ABI indentations can be located on small specimens.

ABI test results from the solder bumps agreed well with those from the tensile specimen shoulders, as shown in Figure 6. Compared with the ABI data from the tensile specimens, the solder bump data showed slightly higher flow stresses and work hardening rate. Also, the yield strength

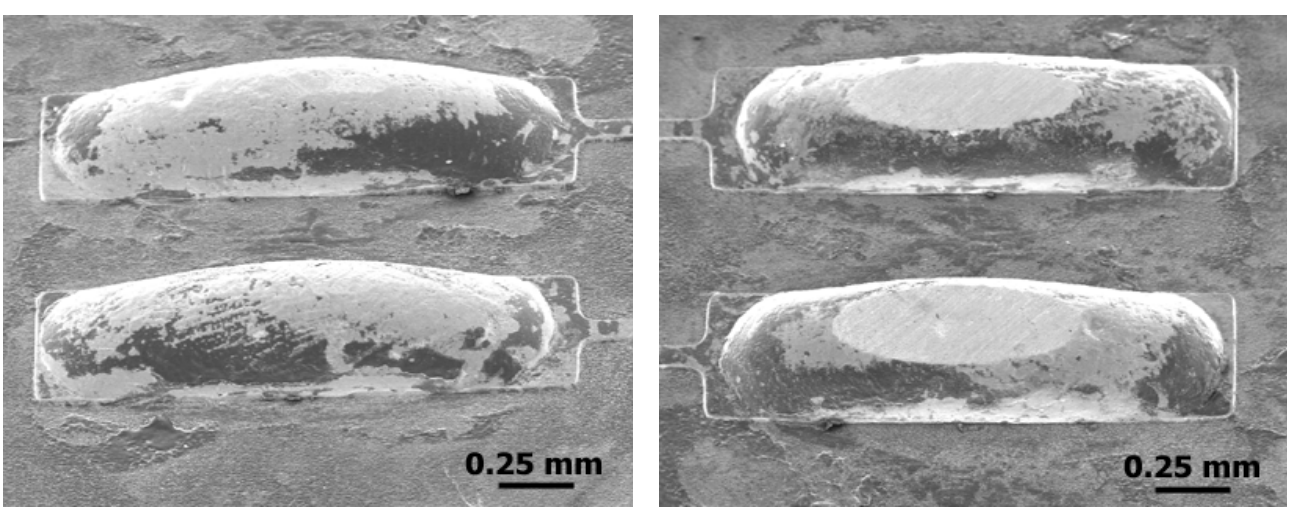

Figure 4. Sn-3.5Ag solder bumps on FR4 test board before (left) and after (right) polishing.

determined for the solder bump was strength determined for the solder bump was higher than that of the bulk alloy. There are a number of possible reasons for the discrepancies between the tensile data and the ABI data sets. Calculation of the yield strength and the flow curve from the ABI data uses empirical constants that are determined from the materials being tested. Confidence in the values of these constants increases proportionately with the amount of available tensile test data and ABI test data. Also, specific tests, which were not performed in this experiment, may be done to determine the values of some of the constants. Another source of error relates to the strain rate sensitivity of the solder alloys, which is relatively high. The strain rate during tensile testing is nearly constant until the onset of necking. However, during ABI testing, the strain rate decreases by over an order of magnitude because of the geometry of the deformation under the indenter. Traditionally, controlling strain rate during ABI testing was not a concern because it is not important for determining the properties of steels.

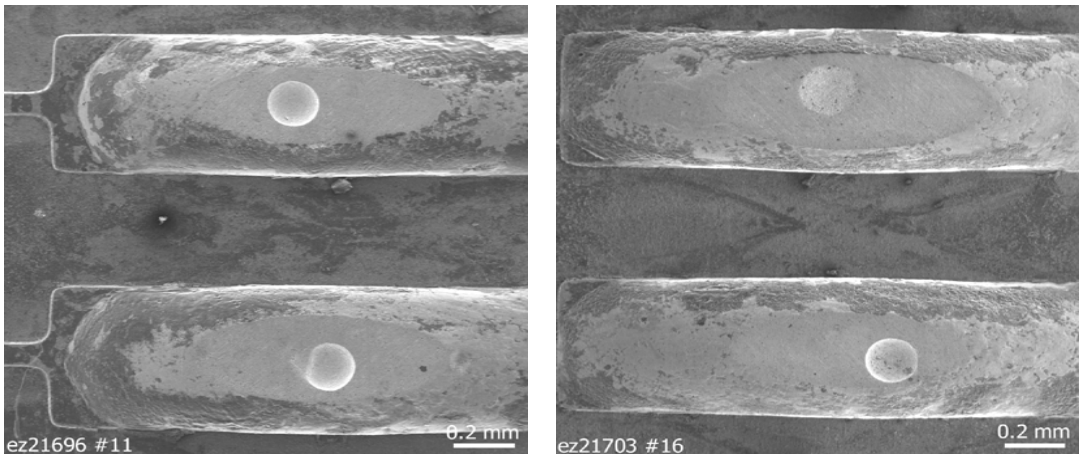

Figure 5. ABI indentations on Sn-3.5Ag solder bumps.

Another source of error in the ABI tests on the solder bumps is defects in the material. A radiograph of the FR4 test board used for this experiment (Figure 7) indicates that most of the bumps contain porosity defects, as indicated by the dark spots. Arrows are used in Figure 7 to indicate the bumps that were ABI tested; while some of the spots are indentations, most of them are porosity defects. Finally, one important difference between the data from the bulk alloy and that from a solder bump (Figure 6) is that the solder bump has chemically reacted with the copper on the test board. It is possible the combined effects of reaction with the Cu and the different thermal processing of the bump produced a measurable difference in properties.

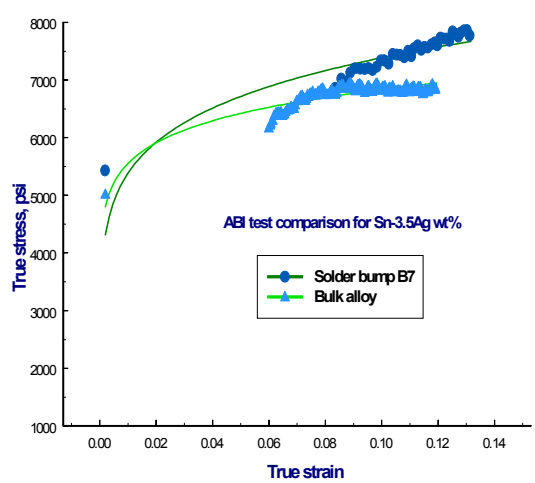

Figure 6. Comparison of ABI results from the bulk alloy and a solder bump of Sn-3.5Ag solder alloy.

These results show that valid ABI tests can be conducted on relatively small volumes of solder alloys, and that the data from such tests agree well with tensile test data from the bulk material. The results indicate the reasonable possibility of obtaining valid tensile property measurements on actual solder joints.

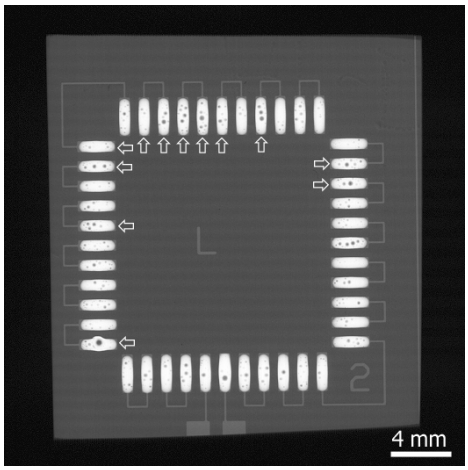

Figure 7. Radiograph of FR4 test PC board used for ABI testing.

4. AUTOMOTIVE INTEGRATED POWER MODULE (AIPM) COMMERCIAL DEVELOPMENT

A. SatCon Automotive Integrated Power Module Program

SatCon Technology Corporation
161 First Street
Cambridge, MA 02142

Objective

The objective of this program is to produce an Automotive Integrated Power Module (AIPM) that meets the technical objectives established by the Electrical/Electronic Technical Team of the PNGV and that can be manufactured at a cost below $0.01 per watt. This is a significant challenge in power electronics and controls design and manufacturing. The benefit of finding the right solution is the promise of a large and lucrative market for IPM products in the future. SatCon Technology Corporation fully appreciates the challenge and envisions a credible solution for the automotive industry, and foresees a significant market opportunity for this technology that extends beyond automotive.

As a result, SatCon has formulated a comprehensive approach to addressing the goals of this program and to actively preparing for the resulting market opportunity. Overall, the strategy was to develop the business of the IPM in concert with the technology and product. In support of this strategy, SatCon set out to find and develop other markets for low cost power electronics in the high same general power class as the AIPM. The central technical goal was developing and validating innovative manufacturing technology to allow the production of low cost, integrated, power modules for the market. To insure success in this challenging effort, SatCon will complement our own technical expertise with that of companies, institutions and individuals recognized for proven electrical component or subsystem design, their product manufacturing, and/or innovative, cost effective process control.

Technical Approach

SatCon's technical approach combines innovation, simplicity, and manufacturability to meet the cost goals. The notional design capitalizes on our considerable experience in power and control electronics advanced design, development and manufacturing. It emphasizes low cost materials and processes, maximum integration of components and maximum efficiency of manufacturing and assembly.

The design of the AIPM must emphasize simplicity, batch processes and testable sub-assemblies. Simplicity reduces parts count, number of process steps and potential for yield loss. Batch processes in place of serial will speed up the build process and reduce the touch labor. The pretestable sub-assemblies keep the yield impact of bad components to a minimum.

Engineered materials have become a baseline for high reliability, high power density power electronics and yet their low volume manufacturing processes has made them unaffordable for most systems. Accordingly, the SatCon design has emphasized the use of conventional materials. The design has also emphasized low total weight since there is a strong correlation between weight and cost in high volume manufacturing costs.

Our program plan combines aggressive technology development to improve performance and reduce manufacturing cost, with extensive prototyping and testing of both technologies and manufacturing processes.

Planned Activities for FY 2000 include program initiation and fundamental technology investigations. The SatCon's program starts with a technology investigation phase of a range of IPM technical issues. These investigations into heat sinks and design approaches, manufacturing technologies, electric power topologies and control hardware and software provide the basis for an interim design for further development. This design along with a series of related manufacturing technology test beds will be built and tested, analyzed, modified and tested again to evolve a more finished product design. The data gathered from this build test build cycle will be used to design a second generation module that will go through the same maturity development cycle before the design is finalized for the end of program.

SatCon started this development program in calendar year 1999 and has made significant progress in technology development and prototyping. During the rest of FY2000, SatCon will continue to develop the technology outlined in proposal design. The planar Generation One prototype Automotive Integrated Power Module (AIPM) design will be tested and various other technical investigations will be evaluated. The analysis carried out during the startup period will be evaluated and a down select of near term technology alternatives carried out. Various test beds will be designed based on the Generation One Prototype and the single-phase test article version. These testbeds will investigate various power IC interconnect technology issues while keeping system complexity and cost down. The results of these test beds will be used to down select processes.

An interim prototype power module based on commercial manufacturing processes for low cost at moderate volumes will be designed as part of the first deliverable prototype to the AIPM program. The intent is to have a design ready for fabrication by the end of this time period and ready for initial testing.

SatCon will also continue to work the production readiness issues in conjunction with ramp up to production of various power electronics products being developed at SatCon or by SatCon subsidiaries.

Anticipated Accomplishments

In FY 2000, SatCon's anticipated accomplishments include the design and fabrication of the interim prototype. This prototype will be delivered to DOE in January 2001 for their

independent evaluation. In addition, the initial advanced technology investigations will be completed and based on their result, critical manufacturing technology demonstrators developed.

B. Power Electronic Building Blocks Drive SPCO's AIPM Development

Dr. Victor A.K. Temple
Senior Vice President, AIPM Program Director and Principal Investigator
Silicon Power Corporation, Commercial Power Division
3 Northway Lane North, Latham, NY 12110

Introduction

SPCO (Silicon Power Corporation) and its team proposes to develop and demonstrate low cost Automotive Integrated Power Modules (AIPM) suitable for mass production, and for a wide range of automotive applications. Its team includes Rockwell Automation, Rockwell Science Center and a large semiconductor manufacturer, MICREL, located in San Jose. SPCO's PEBB technology, MICREL's very large semiconductor manufacturing capability and Rockwell's drive know-how and large commercial market give this team an unbeatable combination of technology, manufacturing and marketing.

The central enabling feature of the SPCO AIPM is a PEBB (Power Electronic Building Block) switch module, which simultaneously slashes production cost and multiplies operating lifetime. These improvements result primarily from two innovations: integrated liquid cooling, which reduces die temperature by providing ultra-low thermal impedance; and installation of the power devices using the thinPak, which dramatically improves thermal cycling capability while minimizing packaging inductance and resistance. Figure 1, below, shows a mock-up of the proposed AIPM.

A secondary benefit of the PEBB switch module, which further reduces cost and improves reliability, is that the control and gate drive system can be simplified by using complementary power devices for the "high-side" switches. Complementary switches are widely used at low voltage, as with the pairing of p and n MOSFETs, but are rarely seen in high power applications because of the lack of suitable p-type switches, until the advent, in 1992, of Harris' first commercial p-type MCT. Complementary switches can be driven from the DC bus rails, eliminating the need for the gate drivers to handle rail-to-rail voltage sluing at very high dV/dt.

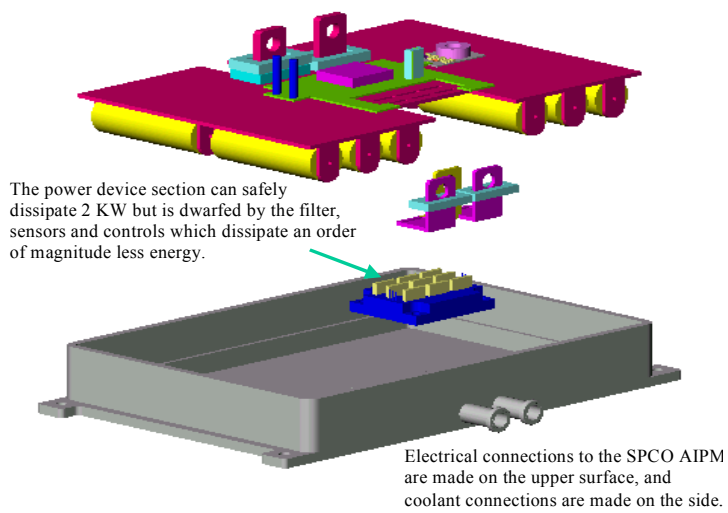

Figure 1: Proposed Pebb-based AIPM. Note that the power switches are dwarfed by the bus, sensors and filter.

Recent Technical Highlights

Technical developments are being carried out by four intercompany teams:

- System Control/Integration
- Inverter Control
- Module/Filter
- Housing/Interface

The system control/integration team is responsible for AIPM design issues involved with interacting with vehicle control and ensuring that the AIPM can carry out the vehicle mission. The inverter control turns system commands into control signals for the power switches using inputs from sensors and feed-back from the power switch modules. The power switch team also includes the bus design as device stresses are strongly related to the details of the filter and bus design. The housing/interface activity is responsible for a housing design that 1) mechanically supports the AIPM's internal blocks, 2) optimally mounts to the vehicle or motor chassis and 3) effectively connects to the battery system, the motor and to vehicle control.

Progress in the first 3 months of this effort include:

- Simulations and device comparison studies that have identified, to first order, the active device switching die area needed to operate at the vehicle's most demanding operating point, namely, 55KW at 200 volt bus voltage. Our team's goal is to be able to operate reliably and indefinitely at this point. This requirement infers that the power device module be able to operate at a dissipation approaching 2 KW with a junction temperature rise that would hold the power device junction temperature within the device's junction temperature rating.

- Identification of PEBB-based advanced IGBT's and MCT's that would result in satisfying AIPM operating requirements with half the silicon of prior standard module technology. It is felt that this is one of the keys to hitting the aggressive cost target of the AIPM program. Figure 2 simulates an SPCO AIPM in which the temperature rise, junction to fluid, is less than 30C for 150W of average dissipation in a single size 9 IGBT. With our pebb based

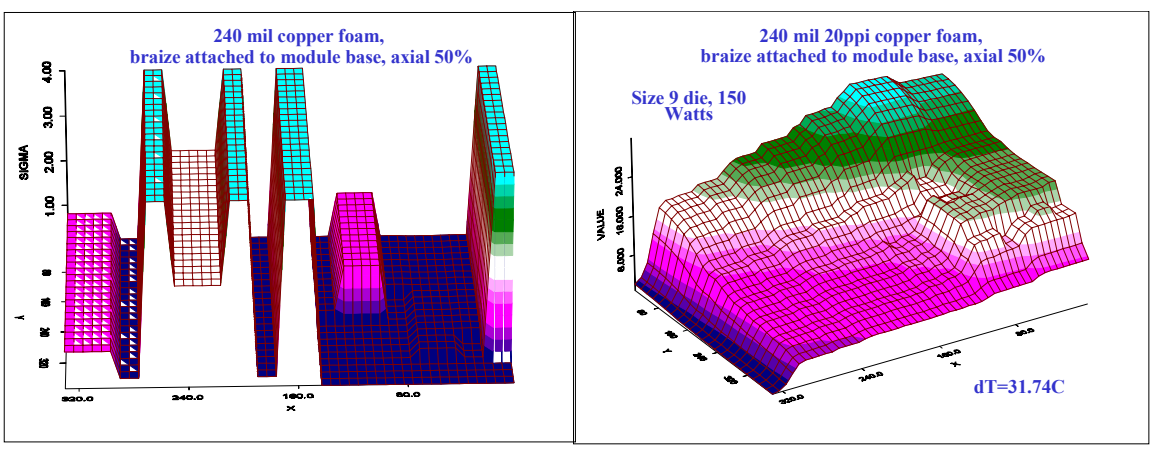

Figure 2. Steady state temperature rise for 150 Watts in a size 9 power device is only 31.74C from junction to fluid.

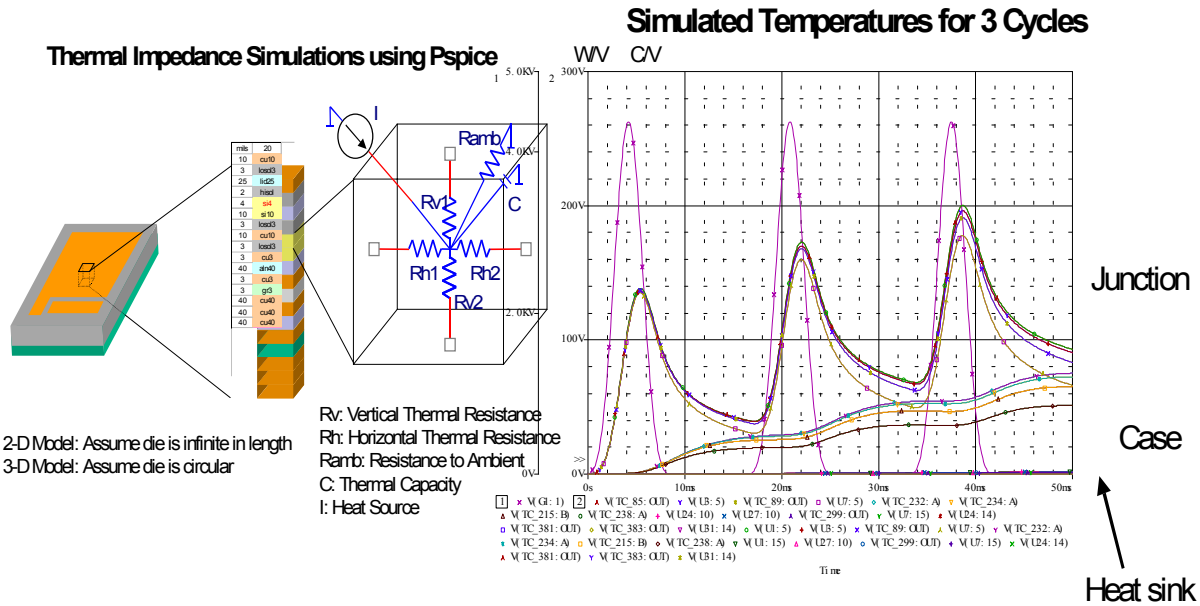

Figure 3. Transient temperature modeling using p-SPICE. Right: sample result for 3 60Hz pulses at 4250 Watts dissipation. Note that the junction temperature is only 100C above its initial temperature at the end of the 3rd pulse. Also note that ~35% of this terrific transient performance is due to the thermal inertia and good attachment of the lid and top copper electrodes.

IGBT (lower Vf and much faster) it appears possible to go from several parallel devices per switch to a single large device per switch. For pulsed operation the power dissipation can be much larger for short periods. Figure 3 shows a calculated result where device dissipation is >4000 watts peak for 3 successive 60 Hz half sine pulses. This simulation is important as this type of rating is important for industrial and commercial drives. In the AIPM it could be used to increase power above 55WK for similar times, perhaps in motor start.

- Innovative packaging technology for at least a factor of two reduction in power module size and contributes to its lower cost. SPCO's thinPak technology seen in Figure 4 eliminates wire bonds, results in near 100% power module yields, reduces parasitics by an order of magnitude and simplifies module manufacturing so that it can be automated as a simple pick and place operation. A device, once thinPak packaged is 100% power testable and can be handled like any surface mount part. But the best news is that modules where thinPak lids replace wire bonds have a 40% reduced mechanical stress leading to orders of magnitude improved temperature cycling life. This is illustrated in Figure 5 that shows that the lid acts as a counterbalance to the ceramic base on which the device is mounted.

- An effective p-type power device, a PEBB innovation that allows the half bridge to be realized without gate drives that are attached to the phase nodes. So, instead of gate drives and floating gate drive power supplies that must bang rail-to-rail at 20 KHz with dv/dt's of 10KV/microsecond, the phase switch high side device gates are referenced to the positive bus. At this time we have only the simulation study to suggest a quantitative advantage from a reliability standpoint, as seen in Figure 6, but the cost advantage is clear in reduced number of gate drives and in their reduced requirements.

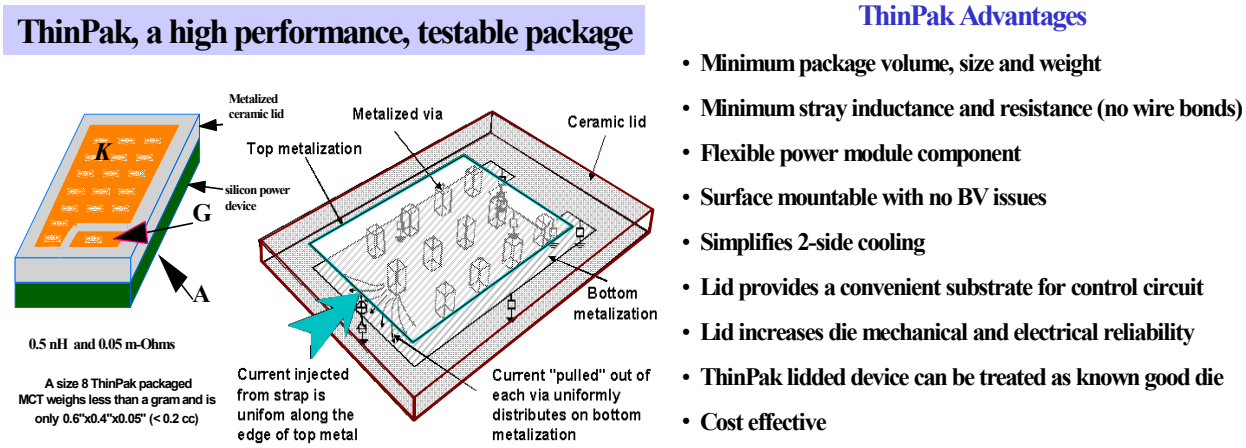

Figure 4. The thinPak uses a 2-side patterned ceramic lid to contact 90% of the power device active area for a very low and extremely high current capability. Record to date: 14,800 amperes for a 0.4 cm2 active area device in conjunction with a 1400V n-type MCT.

Planned Activities

1. Complete initial design study. This study includes complete design comparisons at each stage of traditional vs advanced technology solutions to device, package and cooling issues. Where new technologies are being considered this work will also include reliability studies with an emphasis on experimental results.

Designs will specify issues and developments needed over the next three years to reduce cost. SPCO's chief issues here include silicon cost reduction via process simplification and process yield enhancement. Several "dense channel" size 8 device wafers formerly processed at Harris have yielded at 100%. Package cost reductions promised by thinPak may be put in jeopardy if the cost of the fluid heat exchange is too high. Here we are looking at copper foam as a very low cost possibility but have identified and demonstrated the desired performance with foam from only a single vendor. Our second best alternative is to use AlSiC bases with built-in cone-shaped fins and aluminum nitride device isolation bases. Besides these heat exchange solution, both Rockwell and SPCO are investigating the possibilty of co-

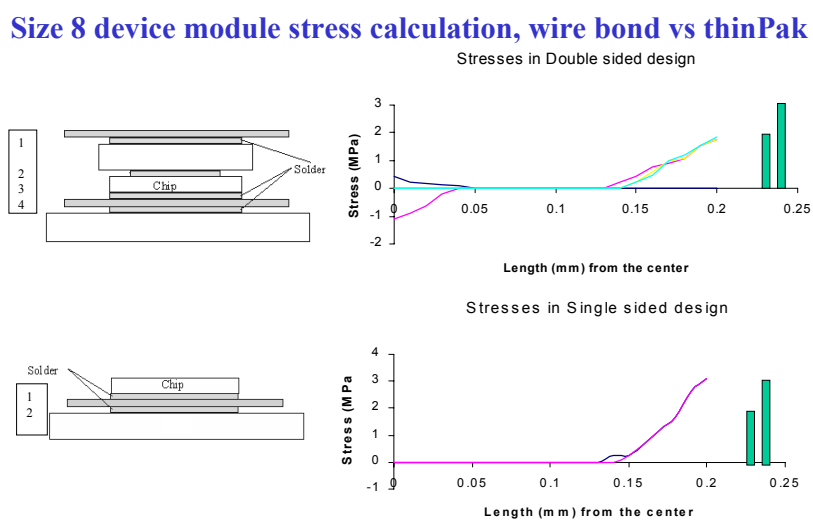

Figure 5. The thinPak lid counterbalances the base for a 40% lower stress, 10x more reliable assembly.

manufacture of these modules produced in flat-base form for standard cooling techniques since it is our team's goal to serve other markets with the AIPM. Our expectation is that with standard air or fluid cooled cold plate heat exchange that the AIPM module will still be able to be rated at at least 25KW.

2. First prototype AIPM module. It will also continue to interact with the AEMD programs directly and with the aid of such software tools as ADVISOR. To better utilize ADVISOR, SPCO and Rockwell plan to generate device and control algorithm specific AIPM models as well as internal models that will allow one to exercise our AIPM while "monitoring" junction temperature and solder layer stresses.

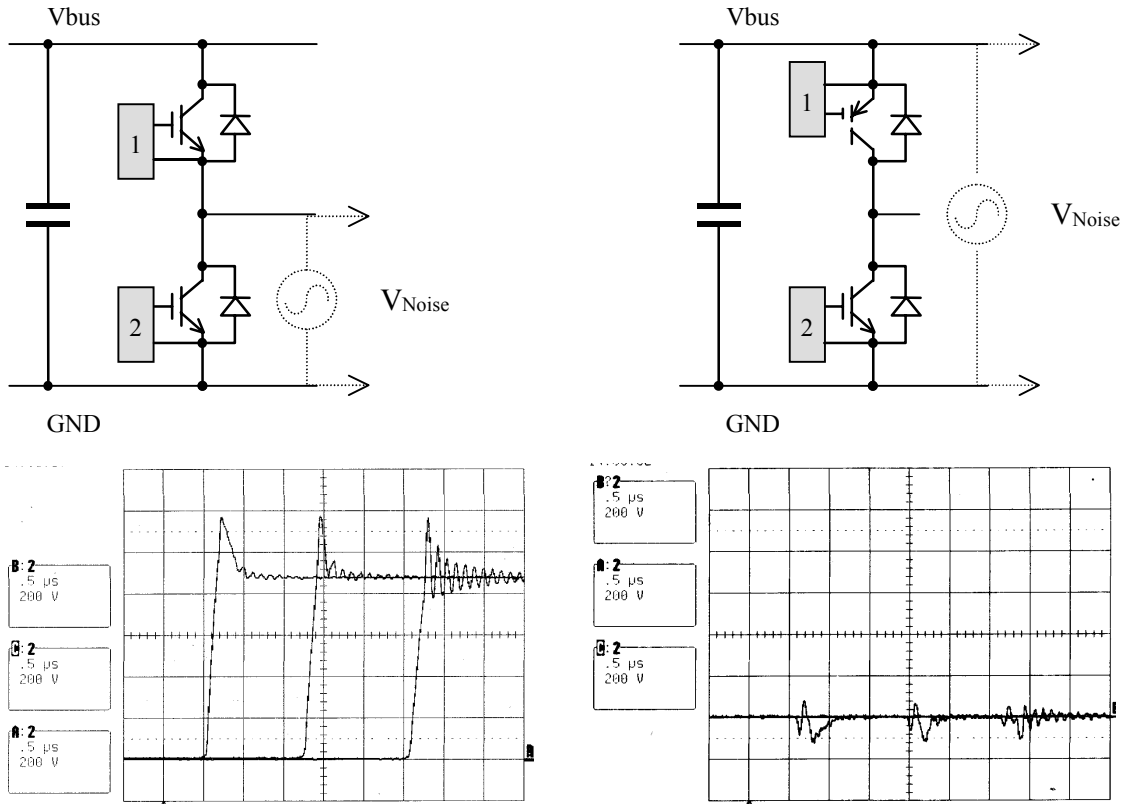

(a) Standard practice with NIGBTs

(b) Suggested structure with PMCTs and NIGBTs

Figure 6. A complementary upper switch reduces cost and reduces noise in the gate drive and control circuits by over an order of magnitude.

5. ELECTRIC MOTOR DRIVE COMMERCIAL DEVELOPMENT

A. Automotive Electric Motor Drive (AEMD) Development

Delphi Automotive Systems
Energenix Center
Kokomo, Indiana

Objectives

- Demonstrate real commercial viability for high volume production and support and integration of the AEMD and other advanced components into PNGV concept vehicle demonstrations.

- Develop designs for high efficiency and low cost 30 kW and 53 kW motor drive systems suitable for hybrid vehicle applications.

- Reduce cost of manufacturing electric motors by 40% to 60% from the present cost of comparable industrial ac motors.

- Develop a drive motor of 10kW to 15 kW range to verify and validate findings.

Approach

- Delphi's focus will be to develop the manufacturing technologies that would potentially reduce the cost of the electric drive systems by 40% to 60%. Delphi will investigate high-rate manufacturing methods for designs incorporating improved laminations, novel heat transfer mechanisms, and packaging to fit the motor within existing vehicle architectures.

- Delphi will also use finite element analysis to evaluate product design concepts.

B. Automotive Electric Motor Drive (AEMD) Development

Delco Remy International
2902 Enterprise Drive
Anderson, Indiana 46013

Objectives

- The primary focus of this effort is cost reduction to produce 30 kW motors for under $450 and 15kW motors for under $300 per unit.

- Leverage advanced technologies such as SEMA (Segmented Electromagnetic Array) technology already in development at VCS.

Approach

- Produce system simulation of series and parallel hybrid electric power trains.

- Make SEMA technology sufficiently robust for the harsh automotive environment and other similar applications. For example, achieve high power densities at crankshaft speeds to avoid the use of precision bearings and gears needed at high motor speeds.

- Develop and test 3 generations of the proof-of-concept series and parallel hybrid traction motors.

- Develop pilot SEMA (Segmented Electromagnetic Array) motor manufacturing cell.

- Develop and test 2 generations of proof-of-product series and parallel hybrid traction motors.

The contract is in place and the team has delivered a management plan to DOE. The project team includes the following partners: Delco Remy International, Inc.; Lynx Motion Technology; Visual Computing Systems; and, Electricore.

APPENDIX: ABBREVIATIONS, ACRONYMS, AND INITIALISMS

ABI	automated ball indentation
AEMD	Automotive Electric Motor Drive
AIPM	Automotive Integrated Power Module
ANL	Argonne National Laboratory
ART	Auxiliary Resonant Tank
BDCM	Brushless DC Machines
BME	base metal
BST	barium strontium titanate
CRADA	Cooperative Research and Development Agreement
CTE	Coefficient of Thermal Expansion
DMIC	Duel Mode Inverter Control
DOE	Department of Energy
EC	Electronic Ceramic
EDC	Electronic Ceramic Device
EMI	Electromagnetic Interference
FE/AFE	ferroelectric/antiferroelectric
FUDS	Federal Urban Driving Schedule
HEV	Hybrid Electric Vehicle
HVAC	Heating Ventilation Air Conditioning
LED	Light-Emitting Diode
LLNL	Lawrence Livermore National Laboratory
MEM	Micro-Electromechanical Machine
MHP	Micro Heat Pipe
MLC	multilayer capacitors
MLCC	multilayer ceramic capacitor
MOCVD	metalorganic chemical vapor deposition
MOSFET	Metal-Oxide-Semiconductor Field-Effect Transistor
MPM	mechanical properties microbe
ORNL	Oak Ridge National Laboratory
OAAT	Office of Advanced Automotive Technologies
PEBB	Power Electronic Building Block
PEEMRC	Power Electronics and Electric Machinery Research Center
PLZT	lead lanthanum zirconate titanate
PM	Permanent Magnet
PMBDCM	Permanent Magnet Brushless DC Machine
PMSM	Permanent Magnet Synchronous Machine
PNGV	Partnership for a New Generation of Vehicles
PWM	Pulse-Width Modulation
RGPMM	Radial Gap Permanent Magnet Motor
SEM	Scanning Electron Microscope
SNL	Sandia National Laboratory
SRM	Switched-Reluctance Motor
SSSI	Soft-Switching Snubber Inverter